



AJPCS

AMET International Journal of
Physical & Chemical Sciences



AMET INTERNATIONAL JOURNAL OF
PHYSICAL AND CHEMICAL SCIENCES

AJPCS

Vol. 4, Issue 1,

2021

ISSN 2395-6275

EDITORIAL

Dear Readers,

We are pleased to launch this issue of *AMET International Journal of Physical and Chemical Sciences*, AJPCS from the department of Chemistry and Physics.

Chancellor

Dr. J. Ramachandran

Pro-Chancellor

Dr. Rajesh Ramachandran

Vice-Chancellor

Col. Dr. G. Thiruvatasagam

Editors-in-Chief

Dr. K.K. Sivakumar, Head, Dept.of Chemistry,
Dr. S. Arjunan, Head, Dept. of Physics

Associate Editor

Dr. M. Subha, Director,
Centre for Internal Publications

Published By

Department of Chemistry, Physics & Centre for Internal Publications

Owned by

Academy of Maritime Education and Training (AMET)
135, East Coast Road, Kanathur-603112,
India, Phone: 044-27472155.

Contents

1. Growth and Characterizations of a New Nonlinear Optical DL-methionine Maleate Single Crystals.....	01
S. Arjunan	
2. Agro wastes and its Activated Carbon in the Removal of Industrial Effluent Heavy Metals.....	08
Sivakumar K.K., Senthil A. and Mahalakshmi S.	
3. Nano based Phase Change Materials for Thermal Storage Applications - A Review.....	25
T.R. Heera and Gengan Saravanan	
4. Recent Trends and Challenges of Lithium Sulphur Batteries.....	32
T.R. Heera, Gengan and Saravanan	
5. Recent trends in Lead-Free Inorganic Pervoskite solar cells: A Brief review.....	39
T.R. Heera and Gengan Saravanan	
6. Waste Management Risks and Opportunities Identification.....	46
Kumar S., Sivakumar K.K. and Senthil A.	
7. A Brief Review on Applications of Ultrasonic Technology in Food Quality Control.....	52
T.R. Heera and Gengan Saravanan	

1. Growth and Characterizations of A New Nonlinear Optical DL-Methionine Maleate Single Crystals

S.Arjunan*

*Department of Physics, AMET University, Chennai.

Abstract

A new DL-methionine maleate (DLMM) was synthesized and bulk crystals were grown by slow evaporation technique in aqueous solution at 42°C. The solubility was determined for various temperatures by gravimetric method. The monoclinic structure of the grown crystal was confirmed by X-ray powder diffraction studies. The presence of functional groups and the formation of compound were confirmed by FT-IR analysis. Thermogravimetric and differential thermal analyses reveal that the compound is thermally stable up to 80°C. UV-VIS absorption study shows no absorption in the entire visible region.

Key words: Organic compounds, Growth from solutions, Solubility

1 Introduction

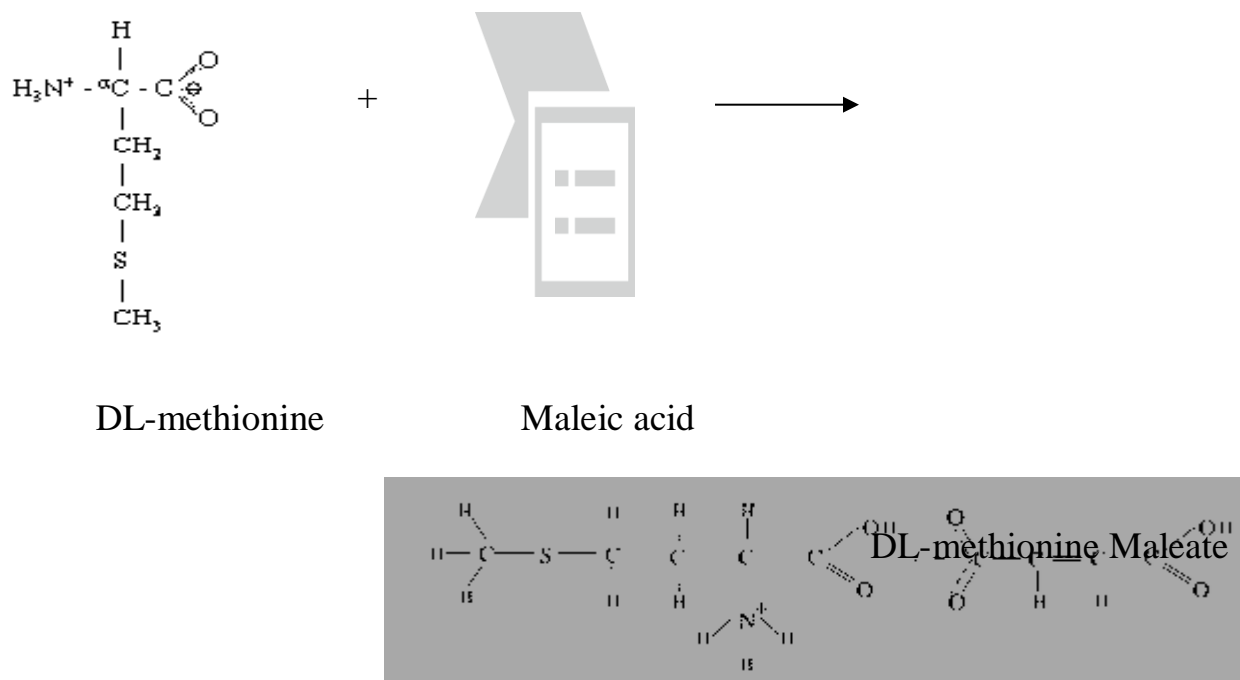
Organic nonlinear optical (NLO) crystals have received considerable attention due to their potential opto-electronic applications such as high speed information processing, optical communications and optical data storage [1-3]. Organic NLO materials are often formed by weak van der Walls and hydrogen bonds and hence they have high nonlinear response and high degree of delocalisation than their inorganic counterparts [4]. Some of the other advantages of organic compounds apart from inherent increased nonlinearity include amenability for synthesis, scope for introducing desirable characteristics by multifunctional substitutions, higher resistance to optical damage and so on. The chirality and hydrogen bonds in organic salts are identified to contribute substantially for remarkable SHG activity [5-6].

Among the organic materials, those based on coulomb interactions between charged molecules often show non-centrosymmetric packing structure, e.g. amino acids, meta nitroaniline (mNA), DAST, etc. Considerable efforts have been made to combine amino-acids with organic acids to produce good optical quality materials as an alternative to the established inorganic materials like KDP. The amino acids combined organic crystals such as L-arginine acetate [7], L-arginine maleate [8], L-threonium acetate [9], L-alanine acetate [10] and L-alaninium maleate [11] have reasonably met the requirements of NLO applications. Organic material DL-methionine maleate [DLMM] has been synthesized from an amino acid

DL-methionine and an organic maleic acid and bulk crystals have been grown from aqueous solution. The growth aspects and the structural, thermal and optical characterizations of DLMM single crystals are presented in this paper.

2 Synthesis and Solubility

DL-methionine maleate was synthesized by dissolving equimolar ratio of DL-methionine and maleic acid in deionized water as per the following reaction.



The synthesized salt was subjected to repeated recrystallization process in order to increase its purity. The recrystallised DLMM salt was used for solubility studies. The solubility was determined for various temperatures (30, 35, 40 and 45°C) by dissolving the solute in 100 ml of deionized water in an air-tight container maintained at a constant temperature with continuous stirring. After attaining the saturation, the equilibrium concentration of the solute was analyzed gravimetrically. The solubility curve for different temperatures is shown in Figure 1. It is observed that the solubility increases with temperature linearly for aqueous solution.

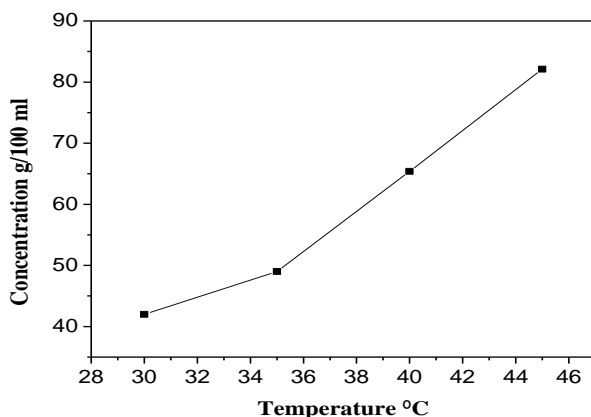


Figure 1 Solubility curve of DLMM in aqueous solution

3 Crystal growth

Based on the solubility data, saturated solution was prepared at 42°C using recrystallised DLMM salt. The solution was kept at this temperature in a constant temperature bath with a temperature accuracy of $\pm 0.01^\circ\text{C}$ achieved by an optical heating arrangement and allowed for slow evaporation. After 20 days, colorless optical quality crystals of maximum dimension $12 \times 4 \times 2 \text{ mm}^3$ have been harvested as shown in Figure 2.

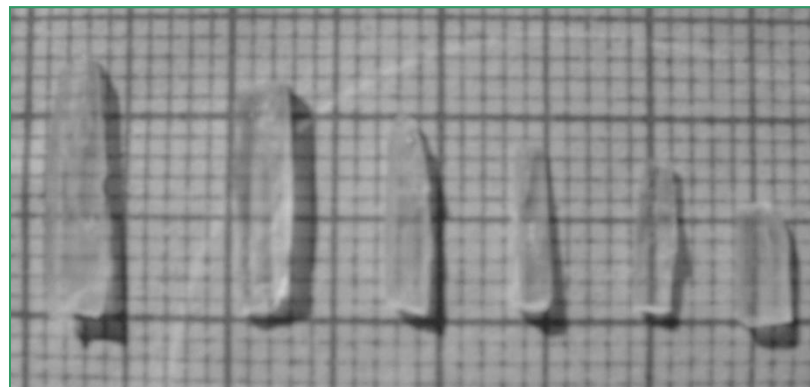


Figure 2 As-grown DLMM crystals by slow evaporation method
over a growth period of 20 days

4 Characterizations studies

4.1 X-ray powder diffraction study

The powdered sample of the grown DLMM crystal was subjected to powder X-ray diffraction study to confirm the crystalline nature of the material. A RICH-SIEFERT powder X-ray diffractometer employing CuK α radiation ($\lambda = 1.5418 \text{ \AA}$) was used to record the spectrum with a scan speed of $2^\circ/\text{min}$. The powder X-ray diffraction pattern of DLMM crystal is shown in Figure 3. The lattice parameter values were calculated to be $a = 11.070 \text{ \AA}$, $b = 5.746 \text{ \AA}$, $c = 19.697 \text{ \AA}$ and $\beta = 102.34$ by least square fit method. This study

confirms that the grown crystal possess monoclinic structure which are in good agreement with reported data [12].

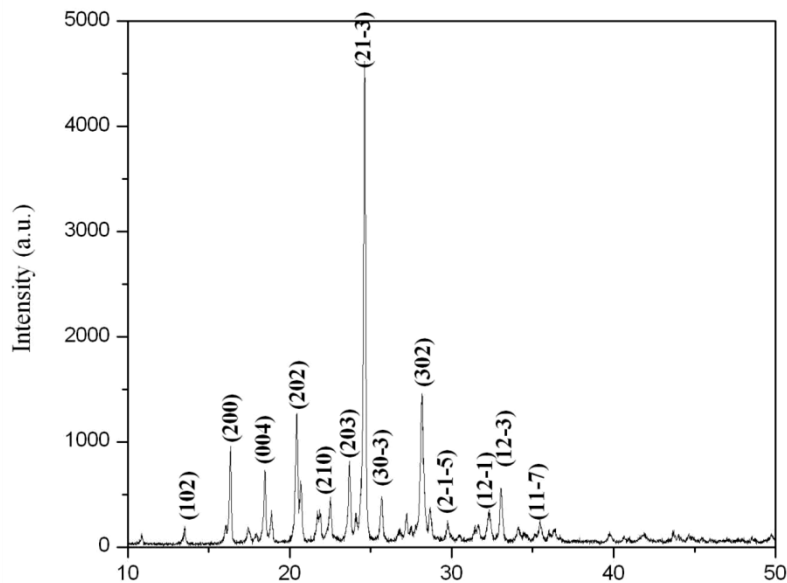


Figure 3 Powder X-ray diffraction pattern of DLMM crystal

4.2 FT-IR study

The presence of functional groups and the formation of compound of DLMM were confirmed by FT-IR analysis. The FT-IR spectrum was recorded in the range 400-4000 cm⁻¹ using PERKIN ELMER spectrometer by KBr pellet technique and the spectrum is shown in Figure 4. The peak at 3423 cm⁻¹ in the higher energy region is assigned to OH stretch of water molecule. The broad band that follows OH stretch of water in the lower energy region includes OH stretch of COOH and NH stretch of NH₃⁺. The peak at 2918 cm⁻¹ is due to CH₂ stretch of DL-methionine. The CH stretch of maleic acid which is supposed to be observed above 3000cm⁻¹ appears to get overlapped with NH and OH stretching vibrations. The band at 1960 cm⁻¹ includes the combination band originating from NH₃⁺ stretching and its torsional oscillations. There are fine structures in the lower energy portion of the envelop which illustrate hydrogen bonding of NH₃⁺ grouping. The C=O stretch of DL-methionine and maleic acid produces its characteristic peak at 1720cm⁻¹. The shoulder that appears in the higher energy portion of the band that lies between 1700and 1350cm⁻¹ is mainly due to OH bending vibration mode and the broad band includesNH₃⁺ symmetric and asymmetric vibrations and C-N vibrations. The sharp peak at 1341 cm⁻¹ is assigned to CH bending vibration and the peaks between 1300 and 900 cm⁻¹ are due to

COO⁻ vibrations. The peak at 553 cm⁻¹ is due to NH₃⁺ torsional oscillations. Thus, the various functional groups in DLMM have been confirmed from this analysis.

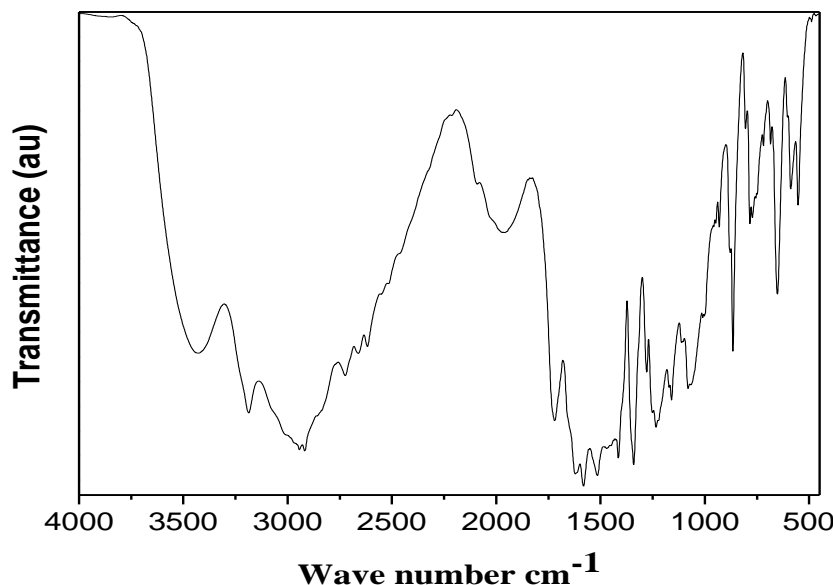


Figure 4 FT-IR spectrum of DLMM

4.3 Optical studies

The UV-VIS absorption spectrum for DLMM single crystal was recorded using SHIMADZU UV-Visible spectrophotometer in 200–1200 nm range as shown in Figure 5. The cut-off wave length is observed at 360 nm from the absorption curve. As there is no absorption in the entire UV-visible region, DLMM is a suitable material for optical applications.

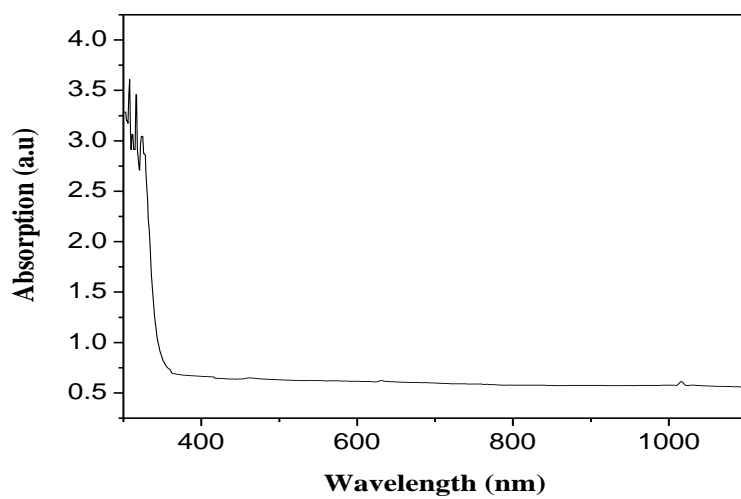


Figure 5 UV-Visible absorption spectrum of DLMM crystal

4.4 Thermal studies

Thermo gravimetric (TGA) and Differential thermo gravimetric (DTA) studies of DLMM were carried out using PERKIN-ELEMER thermal analyzer (STA 409 C) with alumina as reference and TGA curve is shown in Figure 6. There is a sharp weight loss starting at about 80°C, equal to 13.7 %, which is assigned to loss of water of crystallization. The calculations reveal that it is equal to loss of two moles of water. This observation also supports the presence of water in the lattice of DLMM as discussed in FT-IR analysis. This loss of water of crystallization is followed by a major weight loss due to the degradation of DLMM. Hence, this study illustrates that 80°C as the maximum temperature for exploiting DLMM for NLO applications. The DTA curve of DLMM is shown in Figure 7. There are transformations, particularly endothermic, above 100°C. This endotherm appears to have correspondence to TGA result. As there is no endotherm below 117°C, the compound appears to decompose without melting.

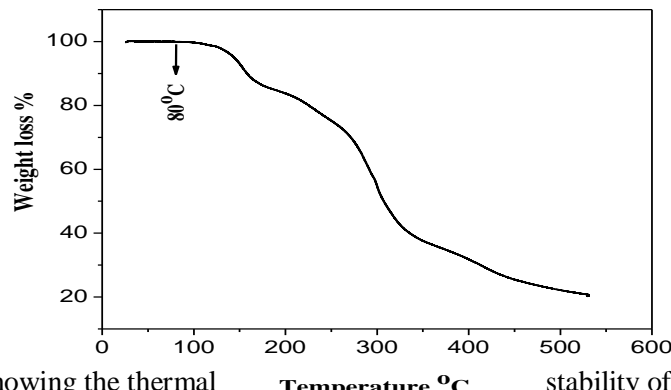


Figure 6 TGA curve of DLMM showing the thermal stability of crystals upto 80°C

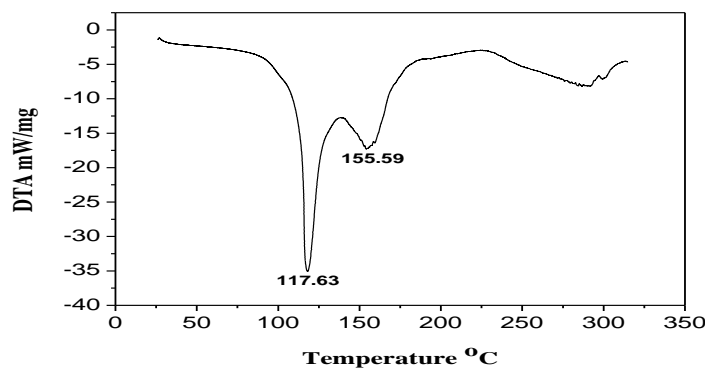


Figure 7 DTA curve of DLMM showing a strong endotherm peak at 117°C

5 Conclusions

Single crystals of DLMM have been grown by slow evaporation technique. The solubility study of DLMM for different temperatures indicates that the solubility increases with temperature linearly in aqueous solution. X-ray diffraction studies revealed the monoclinic structure of the grown crystals. FTIR spectral analysis confirmed the presence of functional groups and the formation of DLMM compound. Optical property studies showed no absorption in the entire visible region. Thermal analyses confirmed that the DLMM is thermally stable up to 80°C. With promising structural, optical and thermal properties, DLMM crystals will be a potential material for optical applications.

REFERENCES

- [1] M.S. Wong, C. Bosshard, F. Pan, and P. Gunter, *Adv. Mater.* 8, 677 (1996).
- [2] S. Chenthamarai, D. Jeyaraman, P.M. Ushashree, K. Meera, C. Subramanian, and P. Ramasamy, *Mat. Chem. Phys.* 64, 179 (2000).
- [3] V.G. Dmotroev, G.G. Gurzadyan, and D.N. Nicogosyan, "Handbook of Nonlinear Optical Crystals", Springer-Verlag, New York, 1999.
- [4] M.N. Bhat, and S.M. Dharmaprkash, *J. Crystal Growth* 236, 376 (2002).
- [5] J. Zyss, J.F. Nicoud, and M. Coquillay, *J. Chem. Phys.* 81, 4160 (1984).
- [6] C. Razzetti, M. Ardoino, L. Zanotti, M. Zha, and C. Pororici, *Cryst. Res. Technol.* 37, 456 (2002).
- [7] R. Muralidharan, R. Mohankumar, R. Jayavel, and P. Ramasamy, *J. Crystal Growth* 259, 321 (2003).
- [8] K. Vasantha, and S. Dhanuskodi, *J. Cryst. Growth* 269, 333 (2004).
- [9] G. Ramesh Kumar, S. Gokul Raj, R. Mohan, and R. Jayavel, *J. Crystal Growth* 283, 193 (2005).
- [10] R. Mohankumar, D. Rajan Babu, D. Jayaraman, R. Jayavel, and K. Kitamura, *J. Crystal Growth* 275, e1935 (2005).
- [11] K. Vasantha, and S. Dhanuskodi, *J. Crystal Growth* 263, 466 (2004).
- [12] M. Alagar, M. SubhaNandhini, R.V. Krishnakumar, and S. Natarajan, *Acta Cryst.* E58, o396 (2002).

2. Agro wastes and its Activated Carbon in the Removal of Industrial Effluent Heavy Metals

Sivakumar K.K.*¹, Senthil A.¹ and Mahalakshmi S.²

^{*1}Department of Chemistry, AMET Deemed to be University, Chennai.

²Arasu Nursing College, Virudhunagar.

ABSTRACT

Heavy metal contamination is considered to be one of the most ubiquitous and complex environmental problems today. An experiment was conducted to ascertain the potential of using Agro-waste (Banana peels) and activated carbon as bio-adsorbent for the removal of Lead, Cadmium, Nickel, Chromium and Zinc from industrial effluent. Parameters such as Percentage dosage, pH, and Temperature were studied. The sample was collected from waste water discharging point at local Paint industries, located at sub urban of Chennai, India. Preliminary screening for heavy metal content indicated that the effluent soil contained 1.2 ± 0.1 mg/L Pb²⁺, 0.42 ± 0.01 mg/L Zn²⁺ and 0.8 ± 0.01 mg/L Cd²⁺. The effluent's Pb²⁺ and Cd²⁺ contents were observed to be above WHO permissible limit for heavy metal content in industrial effluents, but Zn²⁺ content of the same effluent was below the permissible limit. Percentage removal of the test adsorbent sample (banana peels) ranged from 99.67% to 99.90%, which was more than that of activated carbon (69.60% to 83.00%). The percentage removal of both the test adsorbent and the control sample increased with increase in adsorbent dosage, pH and temperature respectively. This study, therefore, suggest that banana peels hold potential to remove heavy metal from industrial waste effluents and could be used as an alternative to remediate environmental pollution problems in the tropics.

Keywords: Agro-waste, Banana peels, industrial effluent, heavy metals.

INTRODUCTION

Heavy metal is any metallic chemical element that is poisonous at low concentrations [1] when consumed over permissible quantities cause psychological disorder [2]. Activated carbon on the other hand, is a term for a family of highly carbonaceous materials none of which can be characterized by a structural formula [3]. The presence of inorganic pollutants such as metal ions

in the ecosystem causes a major environmental problem. Toxic metal compounds coming to the earth's surface not only contaminate earth's water (seas, lakes, ponds and reservoirs), but can also contaminate underground water in trace amounts by leaking from the soil after rain and snow [4]. The numerous metals which are significantly toxic to human beings and ecological environments, include chromium (Cr), copper (Cu), lead (Pb), cadmium (Cd), mercury (Hg), zinc (Zn), manganese (Mn) and nickel (Ni) [5].

Metal ions are released into the environment from many sources [1]. Arsenic is introduced in water through natural and anthropogenic sources: release from mineral ores, probably due to long term geochemical changes and from various industrial effluents like metallurgical industries, ceramic industries, dye and pesticides manufacturing industries and wood preservatives [6]. The major sources of antimony released into the environment through wastewater streams are such industries as lead-storage batteries, soldering, bearing and power transmission equipment, sheet and pipe metals, ammunition, flame retardants, ceramics, casting, enamels, and paints [7]. Wastewaters such as those generated during dyes and pigments production, film and photography, galvanometry, metal cleaning, plating and electroplating, leather and mining may contain undesirable amounts of chromium (VI) anions [8]. Cobalt, which is widely used in alloys (especially magnetic steels and stainless steels), electronics, porcelain and radioisotope therapy, is now commonly found in contaminated water, [9]. Manganese is released into the environment by industries such as those involved in the production of fertilizer, petrochemicals, electroplating, tanneries, metal processing, and mining [10]. Mercury can be found in wastewater discharged from chloro-alkali, paper and pulp, oil refinery, paint, fossil fuel burning, metallurgical processes, pharmaceutical and battery manufacturing [11]. Effluents from production of batteries, gasoline additives, pigments, alloys and sheets etc. contain often high concentrations of lead ions. Mining and metallurgy of nickel, stainless steel, aircraft industries, nickel electroplating, battery and manufacturing, pigments and ceramic industries wastewaters contain high amounts of nickel ions, [7]. Zinc can be found in wastewater from metallurgical processes, galvanizing plants, stabilizers, thermoplastics, pigment formation, alloys and battery manufacturing in addition to the discharges of municipal wastewater treatment plants.

Metal ions are reported as priority pollutants, due to their mobility in natural water ecosystems and due to their toxicity, [12]. The problem associated with metal ions pollution is that they are not biodegradable and are highly persistent in the environment. Thus they can be

accumulated in living tissues, causing various diseases and disorders [13]. Heavy metals toxicity can result in damage or reduced mental and central nervous function, lower energy levels and damage to blood composition, lungs, kidneys, liver and other vital organs. In many countries, more strict legislations have been introduced to control water pollution. Various regulatory bodies have set the maximum prescribed limits for the discharge of toxic heavy metals in the aquatic systems [14].

It is thus a necessity to remove metal ions from wastewater before it can be discharged [12]. In this respect, many physicochemical methods have been developed for the removal of metal ions from aqueous solutions including Precipitation, evaporation, electro deposition, ion exchange, membrane separation, coagulation etc., [15]. However these methods have disadvantages such as secondary pollution, high cost, high energy input and large quantities of chemical reagents or poor treatment efficiency at low metal concentration [16]. It can be said that the conventional methods for metal ions removal from wastewater are limited by technical and economic barriers, especially when concentration of metals in the wastewater is low (<100 ppm) [17]. Therefore the search and development of an efficient and low-cost metal removal processes is of utmost importance. In this endeavor, biosorption has emerged as an alternative and sustainable strategy for cleaning up water [11].

The use of agro-waste to treat sewage and industrial waste water (toxic metal contaminated water) offers an innovative technique that is both efficient and economical. Thus it creates a need for the conversion of agricultural waste to useful and value-added products. A study of published literatures has shown that heavy metal ions can be effectively removed, using plant materials such as empty palm oil fruit bunch, sour chop seed, modified cassava, cassava fiber, coconut shell etc. [18, 19].

Besides the treatment of contaminated water, the use of agro waste proffers a greener and sustainable means of managing waste. The present study therefore sought to evaluate the efficacy of using agro-waste (banana peels) in removing heavy metals from industrial effluent of local Paint industries, Chennai, India.

MATERIALS AND METHODS

Study area

The study was conducted at sur urban industrial complex (SIPCOT), Chennai, India. Chennai is the capital city of Tamil Nadu State in South India. Chennai is located at 13.04°N 80.17°E on the southeast coast of India and in the northeast corner of Tamil Nadu. It is located on a flat coastal plain known as the Eastern Coastal Plains. The city has an average elevation of 6 m (20 ft), its highest point being 60 m (200 ft) is located within the coordinates of 5.5250° N, 7.4922° E, its temperature ranges from 24°C to 39°C.

Biosorbent Sample Collections and Identification

The test sample *Musa sapientum* (banana) peels were collected and sorted from my personal house located in the AMET Deemed to be University, East Coast Road, Chennai.

Sample Preparation

The peels were brought to Chemistry laboratory, Chemistry Department, AMET Deemed to be University, Chennai, where the preparation of the sample and every other analysis were carried out.

In the laboratory the sample was spread on the laboratory work bench and inspected for extraneous materials like insect larva. There after the sample was washed and cut into pieces to increase the surface area for easy drying. Then the pieces sample was oven dried at 100°C for 72hours and dry milled to powdery form, followed by sieving through a sieve of 0.63 to 1.6mm.

The resultant fine sample was collected and soaked in dilute nitric acid solution (2%) for 24hours, filtered and washed repeatedly in distilled water and oven dried at 60°C. Thereafter the sample was rewashed in 1% sodium hydrogen trioxocarbonate (iv) solution to remove any remaining acid, then the sample was washed again with distilled water until pH of 6 was obtained, subsequently the washed sample was dried at 60°C for 5 hours and stored for analysis.

Effluent Collection and Heavy Metal Analysis

The sample was collected from waste water discharging point at Paint industries, located at industrial complex in sub urban of Chennai city. Water sample was collected below the surface using one liter sterile bottle, which has a covering lid. The container was rinsed with water to be sampled, before collection of the sample. Sufficient air spaces were left in the entire bottles to

allowing for expansion of water at increased temperature. The sampling bottle was used directly by holding the bottle horizontally and allowing the water to flow in gently. The bottle was covered, labeled and transported to chemistry laboratory, Chemistry Department, AMET Deemed to be University, East Coast Road, Chennai, India. Trace metals Zn, Cd, Pb, As and Hg in the solutions were determined by Perkin Elmer Atomic Adsorption Spectrophotometer model 238.

Bio-Adsorption with Banana Peel Procedure

Bio-adsorption experiment with the processed sample was conducted to investigate the parametric effects of adsorbate dose, pH and temperature on the adsorption/removal of zinc ion, mercury ion, arsenic ion, cadmium ion and lead ion from contaminated water. 50ml of water sample solution was taken and put in 100ml crew cap conical flask, and specific quantities of test sample (0.1g, 0.3g, 0.5g, and 0.7g respectively) was added separately to the 50ml of the water sample. The mixture was agitated for one hour at 30°C and pH of 6.0. The resultant solution was filtered through 0.45 μ m membrane filter paper. The same procedure was repeated at temperatures of 40°C, 50°C and 60°C, and pH of 5.0, 7.0, and 8.0. The amount of metal ions in aqueous phase was determined by a Perkin Elmer Atomic Adsorption Spectrophotometer model 238. The procedure was once again repeated using activated charcoal as adsorbent, and the result was used as a control.

Statistical Analysis

Data collected were subjected to statistical analysis of ANOVA using statistical analytical system (SAS) software, IBM SPSS statistic 20.

RESULTS

Table 1 shows result of the amount of the heavy metals screened in the industrial effluent studied. From the table it can be observed that there was no trace of mercury and arsenic in the effluent. However, the effluent was discovered to contain 1.12 ± 0.22 mg/L of Pb^{2+} , 0.42 ± 0.05 mg/L of Zn^{2+} and 0.87 ± 0.23 mg/L of Cd^{2+} . The results of amount of Pb^{2+} removed from the effluent or adsorbed by the adsorbents (Banana peel and activated carbon) are shown in table 2 and 3. From the results it can be observed that percentage removal of Pb^{2+} by *Musa sapientum* peels ranges from 99.67 to 99.90, while that of activated carbon ranged from 69.6% to 83.00%. Observations from the tables 2 and 3 shows that percentage removal of the Pb^{2+} metal ion increased as the absorbent dose increased from 0.1g to 0.5g. This is suggested to result from increase in the

absorbing or biding sites as the surface area of the absorbent increases. However, there is a decrease in percentage removal as the absorbent dose increase from 0.5g to 0.7g. This behavior was observed in both *Musa sapientum* peels observed and activated carbon. Tables 4 and 5 contains the results of percentage of Cd²⁺ removal by Banana peels and activated charcoal. From the results, it can be observed that percentage removal of Cd²⁺ by Banana peels ranges from 95.98 to 97.14 in the absorbent dose studied, while activated charcoal ranges from 66.10 to 86.00.

It can be observed that percentage removal in Banana peels and activated charcoal percentage removal increased as the dosage increased from 0.1g to 0.5g but decrease as the dosage increase from 0.5g to 0.7g. Tables 6 and 7 contain the results of removal of Zn²⁺ from the effluent. It can be deduced from the table that the Banana peels removed metal ion Zn²⁺ more than the activated charcoal and further studies on the tables reveal the effect of adsorbent dose on percentage removal of the heavy metals by Banana peels and activated charcoal, shows that both adsorbents behaved as same as regards to dosage effect. Table 8 to13 contain the results of the effect of pH on the removal of heavy metal ions by the test adsorbent studied. A Study of the effect of pH experiments were carried out in the pH range of 5-8 for Pb²⁺, Zn²⁺ and Cd²⁺ with the adsorbent, banana peels and the control activated carbon. Observations from tables 8 through 13 show that the removal of metal ion increased with increasing initial pH of metal ion solution and maximum value was reach at pH 8 for Pb²⁺, Zn²⁺ and Cd²⁺ the increase in percentage removal /adsorption as the solution becomes more alkaline is because of increase in the cations which aids the adsorptions.

The temperature effects on the percentage removal of heavy metal ions by the absorbent studied, are presented in table 14 to 19. Biosorption/removal of heavy metal ions were carried out in different temperatures such as 303⁰C, 313⁰C, 323⁰C and 333⁰C, while other parameters were kept constant. From the results it can be found that percentage removal/biosorption increased with rise in temperature from 303⁰C to 323⁰C in the two test biosorbents, *Musa sapientum* peels and control activated charcoal. As the temperature increases, the rate of adsorbate diffusion across the external boundary layer and in the internal pores of the adsorbate particles as the liquid viscosity decreases with increase in temperature resulting to more adsorption of the adsorbate molecules on the adsorbent surface. On the other hand, as the temperature rises from 323⁰C to 333⁰C there was a decrease in percentage removal or absorption rate. This may be attributed to increase in

temperature which increases the kinetic energy of the metal ions and thus, weakening the forces of attraction between the metal ions and the adsorbent.

Table 1. Heavy metals screening results of the effluent

Heavy metals (mg/L)	Amount	WHO maximum permissible limit
Pb ²⁺	1.21±0.1	0.1
Zn ²⁺	0.42 ± 0.01	1.0
Cd ²⁺	0.87 ± 0.01	0.01
Hg	--	--
As	--	--

Table 2. The effect of adsorbent dose on percentage removal of pb with *Banana* peels

Adsorbent dose (g)	Initial Concentration (Co) (mg/L)	Final Concentration (C ₁) (mg/L)	Co-C ₁ (mg/L)	% Removal (%)
0.1	1.21 ±0.1	0.003873	1.2061	99.68
0.3	1.21 ±0.1	0.002057	1.2079	99.83
0.5	1.21 ±0.1	0.00121	1.2088	99.90
0.7	1.21 ±0.1	0.003993	1.2060	99.67

Table 3. Effect of adsorbent dose on percentage removal of Pb with activated carbon

Adsorbent dose (g)	Initial Concentration (Co) (mg/L)	Final Concentration (C ₁) (mg/L)	Co-C ₁ (mg/L)	% Removal (%)
0.1	1.21 ±0.1	0.3267	0.8833	73.00
0.3	1.21 ±0.1	0.3146	0.8954	74.00
0.5	1.21 ±0.1	0.2057	.0043	83.00
0.7	1.21 ±0.1	0.3678	0.8422	69.60

Table 4.: Effect of adsorbent dose on percentage removal of Cd with banana peels

Adsorbent dose (g)	Initial Concentration (Co) (mg/L)	Final Concentration (C ₁) (mg/L)	Co-C ₁ (mg/L)	% Removal (%)
0.1	0.87 ±1.00	0.035	0.835	95.98
0.3	0.87 ±1.00	0.032	0.838	96.29
0.5	0.87 ±1.00	0.025	0.845	97.14
0.7	0.87 ±1.00	0.029	0.841	96.64

Table 5: Effect of adsorbent dose on percentage removal of Cd with activated carbon

Adsorbent dose (g)	Initial Concentration (Co) (mg/L)	Final Concentration (C ₁) (mg/L)	Co-C ₁ (mg/L)	% Removal (%)
0.1	0.87 ±0.01	0.2949	0.5751	66.105
0.3	0.87 ±0.01	0.1392	0.7308	84.00
0.5	0.87 ±0.01	0.1218	0.7482	86.00
0.7	0.87 ±0.01	0.1054	0.609	70.00

Table 6: Effect of adsorbent dose on percentage removal of Zn with banana peels

Adsorbent dose (g)	Initial Concentration (Co) (mg/L)	Final Concentration (C ₁) (mg/L)	Co-C ₁ (mg/L)	% Removal (%)
0.1	0.42± 0.01	0.0210± 0.01	0.3990	95.01
0.3	0.42± 0.01	0.0182±0.01	0.4018	95.66
0.5	0.42± 0.01	0.0163± 0.01	0.4037	96.11
0.7	0.42± 0.01	0.0215± 0.01	0.3985	94.89

Table 7: Effect of adsorbent dose on percentage removal of Zn with activated charcoal

Adsorbent dose (g)	Initial Concentration (Co) (mg/L)	Final Concentration (C ₁) (mg/L)	Co-C ₁ (mg/L)	% Removal (%)
0.1	0.42 ± 0.01	0.1168± 0.01	0.3032	72.20
0.3	0.42 ±0.01	0.0780± 0.01	0.3410	81.20
0.5	0.42 ± 0.01	0.0689± 0.01	0.3511	83.60
0.7	0.42 ± 0.01	0.1054± 0.01	0.3146	74.90

Table 8: Effect of pH on percentage removal of Pb with banana peels

pH	Initial Concentration (Co) (mg/L)	Final Concentration (C ₁) (mg/L)	Co-C ₁ (mg/L)	% Removal (%)
5.0	1.21 ±0.1	0.00121	1.2088	99.90
6.0	1.21 ±0.1	0.00121	1.2088	99.90
7.0	1.21 ±0.1	0.001089	1.2089	99.91
8.0	1.21 ±0.1	0.000968	1.2090	99.92

Table 9: Effect of pH on percentage removal of Pb with activated charcoal

pH	Initial Concentration (Co) (mg/L)	Final Concentration (C ₁) (mg/L)	Co-C ₁ (mg/L)	% Removal (%)
5.0	1.21 ±0.1	0.2070	1.0030	82.89
6.0	1.21 ±0.1	0.2057	1.0043	83.00
7.0	1.21 ±0.1	0.1980	1.0120	83.64
8.0	1.21 ±0.1	0.1938	1.0162	83.98

Table 10: Effect of pH on percentage removal of Cd with banana peels

pH	Initial Concentration (Co) (mg/L)	Final Concentration (C ₁) (mg/L)	Co-C ₁ (mg/L)	% Removal (%)
5.0	0.87±0.01	0.0249	0.8451	97.14
6.0	0.87±0.01	0.0249	0.8451	97.14
7.0	0.87±0.01	0.00948	0.8605	98.91
8.0	0.87±0.01	0.00870	0.8613	99.00

Table 11: Effect of pH on percentage removal of Cd with activated charcoal

pH	Initial Concentration (Co) (mg/L)	Final Concentration (C ₁) (mg/L)	Co-C ₁ (mg/L)	% Removal (%)
5.0	0.87 ±0.01	0.1371	0.7329	84.24
6.0	0.87 ±0.01	0.1218	0.7482	86.00
7.0	0.87 ±0.01	0.1113	0.7587	87.21
8.0	0.87 ±0.01	0.1044	0.7656	88.00

Table 12: Effect of pH on percentage removal of Zn with banana peels

pH	Initial Concentration (Co) (mg/L)	Final Concentration (C ₁) (mg/L)	Co-C ₁ (mg/L)	% Removal (%)
5.0	0.42±0.01	0.0167	0.4033	96.03
6.0	0.42±0.01	0.0163	0.4037	96.11
7.0	0.42±0.01	0.0134	0.4066	96.81
8.0	0.42±0.01	0.0135	0.4065	96.79

Table 13: Effect of pH on percentage removal of Zn with activated charcoal

pH	Initial Concentration (Co) (mg/L)	Final Concentration (C ₁) (mg/L)	Co-C ₁ (mg/L)	% Removal (%)
5.0	0.42±0.01	0.0705	0.3495	83.22
6.0	0.42±0.01	0.0689	0.3511	83.60
7.0	0.42±0.01	0.0650	0.3550	84.52
8.0	0.42±0.01	0.0630	0.3570	84.99

Table 14: Effect of temperature on percentage removal of Pb with banana peels

Temp (°C)	Initial Concentration (Co) (mg/L)	Final Concentration (C ₁) (mg/L)	Co-C ₁ (mg/L)	% Removal (%)
303	1.21±0.1	0.00872	1.2061	99.68
313	1.21±0.1	0.00872	1.2061	99.68
323	1.21±0.1	0.00872	1.2061	99.68
333	1.12±0.1	0.0120	1.1980	99.01

Table 15: Effect of temperature on percentage removal of Pb with activated charcoal

Temp (°C)	Initial Concentration (Co) (mg/L)	Final Concentration (C ₁) (mg/L)	Co-C ₁ (mg/L)	% Removal (%)
303	1.21 ±0.1	0.2057	1.0043	83.00
313	1.21 ±0.1	0.1908	1.0192	84.23
323	1.21 ±0.1	0.1817	1.0283	84.98
333	1.21 ±0.1	0.1842	1.0258	84.78

Table 16: Effect temperature on percentage removal of Cd with banana peels

Temp (°C)	Initial Concentration (Co) (mg/L)	Final Concentration (C ₁) (mg/L)	Co-C ₁ (mg/L)	% Removal (%)
303	0.87±0.01	0.0249	0.8451	97.14
313	0.87±0.01	0.0257	0.8443	97.05
323	0.87±0.01	0.0208	0.8692	97.61
333	0.87±0.01	0.0215	0.8484	97.52

Table 17: Effect of temperature on percentage removal of Cd with activated charcoal

Temp (°C)	Initial Concentration (Co) (mg/L)	Final Concentration (C ₁) (mg/L)	Co-C ₁ (mg/L)	% Removal (%)
303	0.87±0.01	0.1218	0.7482	86.00
313	0.87±0.01	0.1171	0.7529	86.54
323	0.87±0.01	0.1130	0.7570	87.01
333	0.87±1.00	0.1138	0.7562	86.92

Table 18: Effect of temperature on percentage removal of Zn with banana peels

Temp (°C)	Initial Concentration (Co) (mg/L)	Final Concentration (C ₁) (mg/L)	Co-C ₁ (mg/L)	% Removal (%)
303	0.42±0.01	0.0164	0.4037	96.11
313	0.42±0.01	0.0146	0.4054	96.52
323	0.42±0.01	0.0127	0.4073	96.98
333	0.42±0.01	0.0198	0.4002	95.29

Table 19: Effect of temperature on percentage removal of Zn with activated charcoal

Temp (°C)	Initial Concentration (Co) (mg/L)	Final Concentration (C ₁) (mg/L)	Co-C ₁ (mg/L)	% Removal (%)
303	0.42±0.01	0.0689	0.3511	83.60
313	0.42±0.01	0.0672	0.3528	84.01
323	0.41±0.01	0.0654	0.3546	84.43
333	0.42±0.01	0.0672	0.3528	86.00

DISCUSSION

The present study has established that effluent obtained from local paint industries is polluted with regards to Pb²⁺ and Cd²⁺ but not polluted with regards to Zn²⁺. This conclusion was drawn from comparing the amount of the metal ions found in the effluent studied with the WHO/EPA heavy metal ions permissible limits in industrial effluents. In the present study test results, reveals that the effluent is polluted with Pb²⁺ and Cd²⁺. As this heavy metal contaminated (polluted) effluent is continuously discharged into the environment it will definitely result to soil pollution, and if the effluent ends up in water body it leads to water pollution thereby endangering aquatic and terrestrial lives within the environment. Hence the need to treat the effluent before discharge.

pH of the medium plays a critical role in the process of metal adsorption from an aqueous solution. The solution pH is capable of influencing the dissociation state of the adsorbents, ionic state of functional groups and species of metals. As posited by the effect of pH on solution chemistry of the target metal includes hydrolysis, complexation by organic and/or inorganic ligands and redox potentials. At elevated pH values, adsorption is reduced due to high precipitation, ion exchange and aqueous metal hydroxide formation.

Based on the results of their study, reported that Cu²⁺ adsorption onto banana peel was relatively quicker than those reported for some other bio-adsorbents. They observed a rapid adsorption during the first 30 min, followed by a constant rate of Cu²⁺ removal for further 30 min before reached the equilibrium. In the case of arsenic reported that the equilibrium was established within 30 min, and 75% and 95% sorption was recorded for As(III) and As(V), respectively. According to them, no significant increase in the percent sorption onto banana peel was observed

after 30 min. When particles of banana peel were introduced to the solution, metal ions could find flurry of vacant active binding sites resulting in rapid initial adsorption. This was further confirmed by the adsorption of Pb^{2+} , Cu^{2+} , and Cr^{3+} by five plant materials. According to them, the maximum removal of three metals was attained after a shaking period of 90 min. Once the majority of binding sites were occupied, formation of repulsive forces between the metal ions on the solid surface and the liquid phase makes it difficult for further binding to the remaining vacant surface sites.

It is well understood that the amount of metal removal is vastly dependent upon the metal concentration in the solution. The effect of initial concentration of Cr^{3+} on adsorption by wheat straw, the adsorption rate was increased with the increase in the initial metal ion concentration. However, if the amount of biomass remains constant in the system, the metal removal efficiency may be reduced regardless the increased metal concentration. Furthermore, Cu^{2+} adsorption by banana peel reported that the adsorbent dose is also decisive for metal removal, the highest Cu^{2+} removal (88%) when the initial Cu^{2+} concentration of 10 mg/L with the adsorbent dose of 5 g/L. The effect of adsorbent dosage on the adsorption of Cd^{2+} and Pb^{2+} and the dosages of banana peel ranging 10-90 g/L, and the maximum removal was observed at the doses of 30 and 40 g/L, respectively, for Cd^{2+} (89.2%) and Pb^{2+} (85.3%). At the high doses of adsorbent, removal of metal may be affected by the partial aggregation among the available active binding sites whereas at low doses, lack of active binding sites may result in lower rate of metal removal.

The biosorbent derived from banana peel to study the removal of Cd^{2+} from aqueous solution and reported that particle size of banana peel had no effect on the removal of metal ions, which is analogous to the effect of particle size on uranium and cadmium biosorption by Sargassum biomass. Three sizes of biomass (0.5-0.7 mm, 1.0-1.4 mm and native whole seaweed for uranium; 0.5-0.7 mm, 0.84-1.00 mm and 1.0-1.4 mm for cadmium). According to them, no significant difference in sorption rate for the metals among the tested particle sizes was observed. Cossich et al. (2002), based on their finding with biosorption of chromium onto Sargassum biomass also reported that the rate of biosorption was independent from the particle size of the biomass. [27] further stated that the higher biosorption level achieved by smaller particle size of the biosorbents may not be connected to the fact that smaller particle sizes give large surface areas. However, adsorption is considered to be a surface phenomenon; thus sorbents with higher surface area should exhibit a rapid adsorption than that of sorbents with lower surface area. Furthermore, as stated by [28] the smaller particles do have higher specific surface area and low mass transfer

resistance than the larger biosorbents. In fact, it is observed higher adsorption rate and uptake from the smaller and fine particles of the activated carbon adsorbent prepared from biomass than the larger particles of the same adsorbent [29].

CONCLUSION

From the present study, it was deduced that industrial effluent from Paint industries contain some concentrations of heavy metals such as Pb^{2+} , Cd^{2+} and Zn^{2+} . However, the effluent was significantly polluted with Pb and Cd; and it was also gathered from the study that Agro waste Musa sapientum peels (Banana peel) can be effectively use to treat heavy metal contaminated industrial effluent before discharge to the environment. However, it is more effective with increase in temperature, pH and adsorbent dosage. To this end, Musa sapientum peels are encouraged to be used for industrial effluent discharge treatment

REFERENCES

1. K. Chojnacka . Biosorption of Cr(III) ions by wheat straw and grass: a systematic characterization of new biosorbents. *Pol. J. of Environ. Stud.* 2006; 15:845–852.
2. A. Shafaghat F. Salimi M. Valiei J. Salehzadeh M. Shafaghat . Removal of heavy metals (Pb^{2+} , Cu^{2+} , and Cr^{3+}) from aqueous solutions using five plants materials. *Afr. J. Biotechnol.* 2012; 11:852–855.
3. A.A.M. Daifullah B.S. Girgis H.M.H. Gad . A study of the factors affecting the removal of humic acid by activated carbon prepared from biomass material. *Coll. Surf.* 2004; 235:1–10.
4. Abu Hasan H, Abdullah SRS, Kofli NT, Kamarudin SK. 2012) Isotherm equilibria of Mn^{2+} biosorption in drinking water treatment by locally isolated *Bacillus* species and sewage activated sludge. *J Environ Manage*;111:34-43.
5. Ahmaruzzaman M., (2011) Industrial wastes as low-cost potential adsorbents for the treatment of wastewater laden with heavy metals. *Adv Colloid Interface Sci* 2011; 166:36-59.
6. Alomá I, Martín-Lara M a., Rodríguez IL, Blázquez G, Calero M. (2012), Removal of nickel (II) ions from aqueous solutions by biosorption on sugarcane bagasse. *J Taiwan Inst Chem Eng*;43:275.81

7. B. Volesky . Sorption and Biosorption. BV Sorbex;Montreal, Canada: 2003.
8. Demirbas A. (2008), Heavy metal adsorption onto agro-based waste materials: a review. *J Hazard Mater*;157:220-229.
9. Ding Y, Jing D, Gong H, Zhou L, Yang X. (2012), Biosorption of aquatic cadmium (II) by unmodified rice straw. *Bioresour Technol*;114:20.
10. E.S. Cossich C.R.G. Tavares T.M.K. Ravagnani . Biosorption of chromium(III) by Sargassum sp. biomass. *Electron. J. Biotechnol.* 2002; 5:133–137.
11. El-Shafey EI. (2010) Removal of Zn(II) and Hg(II) from aqueous solution on a carbonaceous sorbent chemically prepared from rice husk. *J Hazard Mater*;175:319-27.
12. EPA, (2013) National Primary Drinking Water Regulations: List of Contaminants and their Maximum Contaminant Levels (MCLs). updated on June. 2013
13. Flores-Garnica JG, Morales-Barrera L, Pineda-Camacho G, Cristiani-Urbina E. (2013) Biosorption of Ni(II) from aqueous solutions by Litchi chinensis seeds. *Bio-resource Technol*;136C:635-643.
14. Guo W, Chen R, Liu Y, Meng M, Meng X, Hu Z, (2013), Preparation of ion-imprinted mesoporous silica SBA-15 functionalized with triglycine for selective adsorption of Co(II). *Colloids Surfaces A Physicochem Eng Asp*;436:693-703.
15. Iqbal M, Saeed A, Edyvean RGJ. (2013), Bio-removal of antimony (III) from contaminated water using several plant wastes: Optimization of batch and dynamic flow conditions for sorption by green bean husk (*Vigna radiata*). *Chem Eng J*;225:192-201.
16. Anwar J, Shafique U, Zaman W. M. Salman A. Dar S. Anwar . Removal of Pb(II) and Cd(II) from water by adsorption on peels of banana. *Bioresour. Technol.* 2010; 101:1752–1755
17. Sivakumar K.K. and Dheenadayalan M.S. (2012) Distribution of heavy metals profile in water and soil system at Amaravathi river basin of Karur, Tamil Nadu, Ind. *J. Envl Prot.* Vol. 32(2).
18. Kýlýç M, Kýrbýyýk Ç, Çepelioðullar Ö, Pütün A.E. (2013), Adsorption of heavy metal ions from aqueous solutions by bio-char, a by-product of pyrolysis. *Appl Surf Sci*;283:856-62.

19. M. Achak A. Hafidi N. Ouazzani S. Sayadic L. Mandi . Low cost biosorbent banana peel for the removal of phenolic compounds from olive mill wastewater: Kinetic and equilibrium studies. *J. Hazard. Mater.* 2009; 166:117–12
20. M. Zhou Y. Liu G. Zeng X. Li W. Xu T. Fan . Kinetic and equilibrium studies of Cr(VI) biosorption by dead *Bacillus licheniformis* biomass. *World J. Microbiol. Biotechnol.* 2007; 23:43–48.
21. M.A. Hossain H.H. Ngo W.S. Guo T.V. Nguyen . Removal of copper from water by adsorption onto banana peel as bioadsorbent. *Int. J. Geomate.* 2012; 2:227–234.
22. Meena AK, Kadirvelu K, Mishraa GK, Rajagopal C, Nagar P.N., (2008), Adsorption of Pb(II) and Cd(II) metal ions from aqueous solutions by mustard husk. *J Hazard Mater*;150:619-25.
23. Mornison G., Fatoki, O., Linder S. and Lundehn C. (2004) Determination of heavy metal concentrations and metal fingerprints of sewage sludge from easterncape Pounce South Africa by ICP-MS and LA-ICP-MS Water Air Soil pollution: 152-111-127
24. N. Fiol I. Villaescusa M. Martinez . Sorption of Pb(II), Ni(II), Cu(II), and Cd(II) from aqueous solution by olive stone waste. *J. Sep. Purif Technol.* 2006; 50:132–140.
25. P. Kaewsarn W. Saikaew S. Wongcharee . Dried biosorbent derived from banana peel: A potential biosorbent for removal of cadmium ions from aqueous solution. In : Proceedings of the 18th Thailand Chemical Engineering and Applied Chemistry Conference; October 20-21, 2008; Pattaya, Thailand. 2008.
26. Sivakumar K.K and Mahalakshmi S. (2008) Kinetics of removal of 2,4-D from aqueous solution by agricultural waste products, *Ind. J Envl. Prot.* 18(9), 399-403.
27. Ramesh, P., Damodhram R. (2016) Determination of heavy metal in industrial waste water of Thrupati Region Andhra Cd 10, U, who 2013 Pradesh 5 (5) International Journal of Science and Research.
28. Rao RAK, Ikram S. (2011) Sorption studies of Cu (II) on gooseberry fruit (*emblica officinalis*) and its removal from electroplating wastewater. *Desalination*; 277:390-398.
29. S.Q. Memon M.I. Bhander J.R. Memon . Evaluation of banana peel for treatment of arsenic contaminated water. In : Proceedings of the 1st Technical Meeting of Muslim Water Researchers Cooperation (MUWAREC); December 2008; Malaysia

3. Nano based Phase Change Materials for Thermal Storage Applications - A Review

T.R.Heera and Gengan Saravanan

^aDepartment of Chemistry, AMET University, Chennai, Tamil Nadu, India

^{b,*} Department of Chemistry, Koneru Lakshmaiah Education Foundation, Hyderabad-500075, Telangana, India. E-mail: saravanan3che@gmail.com; saravanan@klh.edu.in

Abstract

Conventional thermal energy storage systems have low energy storage densities and are incapable of undergoing isothermal storage process. Phase Change Materials (PCMs) are gaining attention as potential materials for thermal energy storage from intermittent renewable energy sources. Latent heat storage materials (LHS) called PCMs can release or absorb heat energy when a change in physical state occurs. Although PCMs have high energy storage density, their poor thermal conductivity remains a challenge in practical applications. Research efforts to combat the low thermal conductivity of PCMs has led to inclusion of nanoparticles in PCM matrix. The thermal conductivity of PCM containing materials can be tuned by nanoencapsulation in PCM matrix. The inclusion of nanoparticles in PCM matrix has been found to significantly improve the heat transfer mechanisms during charging and discharging cycles. This chapter throws light on the recent significant advances in nano based PCM that can be employed for thermal energy storage applications. In addition, the research gaps in enhancing the efficiency of PCM are discussed and certain suggestions for future works in this direction are provided.

Keywords: *Latent heat storage materials; Phase change materials; SWCNT; MWCNT; Graphene.*

1. Introduction

The fast-depleting fossil fuels, rising global temperature and ever-increasing energy demands has made researchers to focus on developing renewable energy technologies. This led to exponential progress in the development of various low carbon strategies and technologies for efficient utilization of non-conventional energy sources during the past decades. However, the fluctuating nature of the renewable energy sources like wind power and solar power poses a challenge for their widespread application. In order to circumvent this issue of intermittent renewable energy

sources researchers have made multiple energy storage technologies such as chemical energy storage, thermal energy storage, electrical energy storage, electro-mechanical energy storage, electro-chemical energy storage.

Thermal energy storage systems play an important role in maintaining an energy demand balance on a daily, weekly or seasonal basis by utilizing renewable energy sources and industrial waste heat recovery. Thermal energy storage is classified into three major types such as Thermo-Chemical Energy Storage (TCS), Latent Thermal Energy Storage (LTES) and Sensible Thermal Energy Storage (STES). In recent years, thermal energy storage systems utilizing phase change materials (PCMs) to store heat in the form of latent heat is attracting considerable interests among researchers worldwide. High technical feasibility, compact size and large energy densities are the advantages of latent thermal energy storage systems. Currently, thermal energy storage systems based on STES are commercially available whereas the TCS and LTES based systems are widely investigated and still in developmental stage.

This paper focusses on the recent developments in the PCM based latent thermal energy storage systems that employs nanoparticles for enhancing the thermal conductivity. The unique electrical properties of nano sized particles when included in PCM matrix has been found to tune the thermal behavior of materials containing PCM. This chapter intends to offer the readers an overview of the most significant research outcomes reported in recent years by introducing various nanoparticles into PCM matrix for tuning thermal conductivity.

2. Phase Change Materials

Latent heat storage using phase change materials is a vital strategy to store heat energy. Phase change materials have the unique ability to absorb or release heat energy during a change in physical state such as solid-liquid or liquid-gas vice-versa. PCM materials generally possess low melting point and absorption of latent heat from the system leads to change in phase without affecting the temperature of the system.

2.1 Significance of phase change materials in LTES

The application of phase change materials in LTES provides isothermal behavior during charging/discharging cycle and greater heat storage capacity as compared to sensible heat storage. High power capacity during charging and discharging cycles and high storage density are desirable

properties of any thermal storage systems. The high energy density of PCM makes PCM based LTES smaller in size and compact as compared to STES. Also, the isothermal behavior during charging/discharging cycles makes PCM based LTES suitable for applications involving a minimum temperature variation.

2.2 Classification of Phase Change Materials

Phase change materials can be divided into three main groups based on their composition and phase change temperature (PCT). Figure 1 depicts the classification of PCM into eutectic, organic and inorganic materials. Based on their melting temperatures PCM have been classified as those materials for solar heating and similar applications ($15^{\circ}\text{C} < T_m < 90^{\circ}\text{C}$), air conditioning applications ($T_m < 15^{\circ}\text{C}$), absorption refrigeration applications ($T_m > 90^{\circ}\text{C}$).

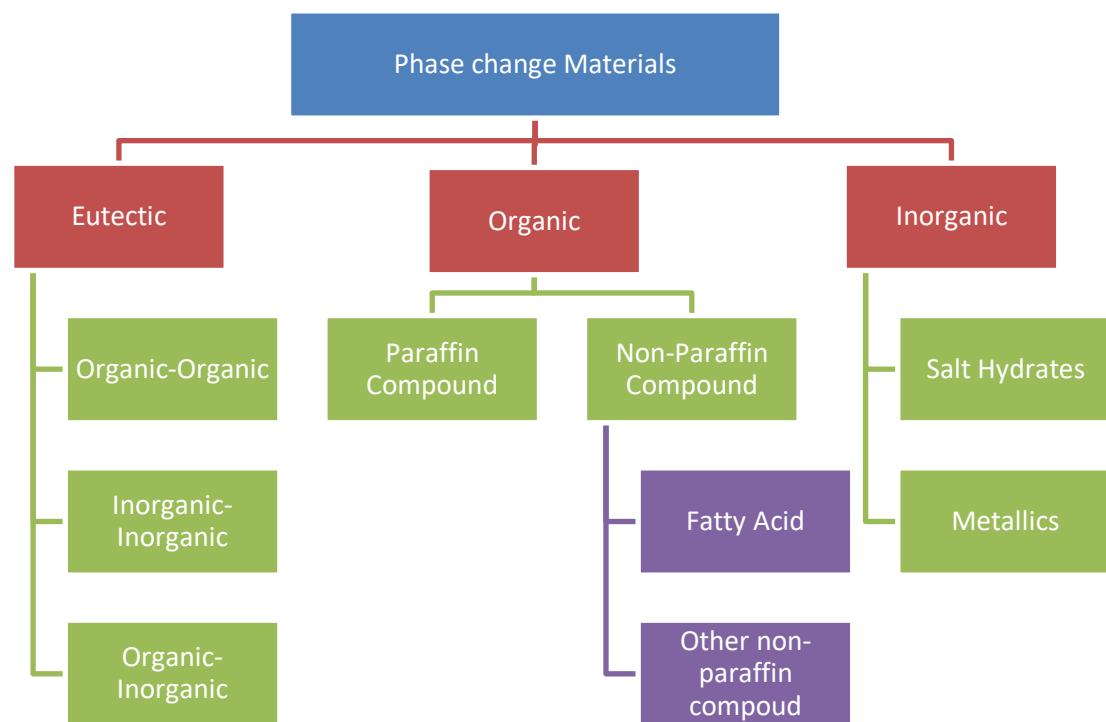


Figure 1: Classification of PCMs (J. Jaguemon et al, 2018)

2.3 Challenge of low thermal conductivity of PCM

The low thermal conductivity of PCM is one of the key issues restricting its widespread applications. The low thermal conductivity of PCM leads to super heating of the liquid phase when exposed to excessive heat loads although most of PCM still remains in solid phase. Improving the thermal conductivity of PCM will enhance the rate of charging and discharging which in turn can help in boosting the efficiency of PCM based LTES.

3. Role of Different Nanoparticle additives

3.1 Carbon nanomaterials

Carbon nanomaterials find extensive application as nanoparticle additives in PCM due to their unique properties. Carbon nanoparticles have high stability, low density and high thermal conductivity. Carbon nanoparticles that are commonly used are single-wall carbon nanotube (SWCNT), multi-wall carbon nanotube (MWCNT), graphene and graphite (Fig.2). In the year 2015, Y.B. Tao, C.H. Lin and Y.L. He revealed that the mass fractions of carbon nanoparticles play an important role in tuning the specific heat capacity and thermal conductivity behavior of PCM based composites in LTES.

Research conducted by Soha Hashempour and Mohammad Hassan Vakili (2018) using different surfactants to stabilize the nanoparticles showed that thermal conductivity of modified MWCNT showed maximum enhancement in butyl stearate.

Graphene is the most significant carbon-based nanomaterial that can be employed to enhance the thermal conductivity of PCMs. Zou et al. (2018) reported the results exhibiting the comparison of PCMs with CNTs and graphene. The results proved the higher capability of graphene compared to CNT to enhance thermal conductivity of PCMs.

Saeed Ranjbar, Hamid Masoumi, Ramin Haghghi Khoshkho and Mojtaba Mirfendereski, (2019) investigated the stability of functionalized and pristine MWCNTs in PCMs with different polarity levels. It was observed that the thermal conductivity improved in all the PCMs with addition of nanoparticles. Amir Al-Ahmed et al (2020) studied the thermal conductivity properties of Octadecanol-MWCNT composite PCMs and identified the composite as promising organic thermal storage material.

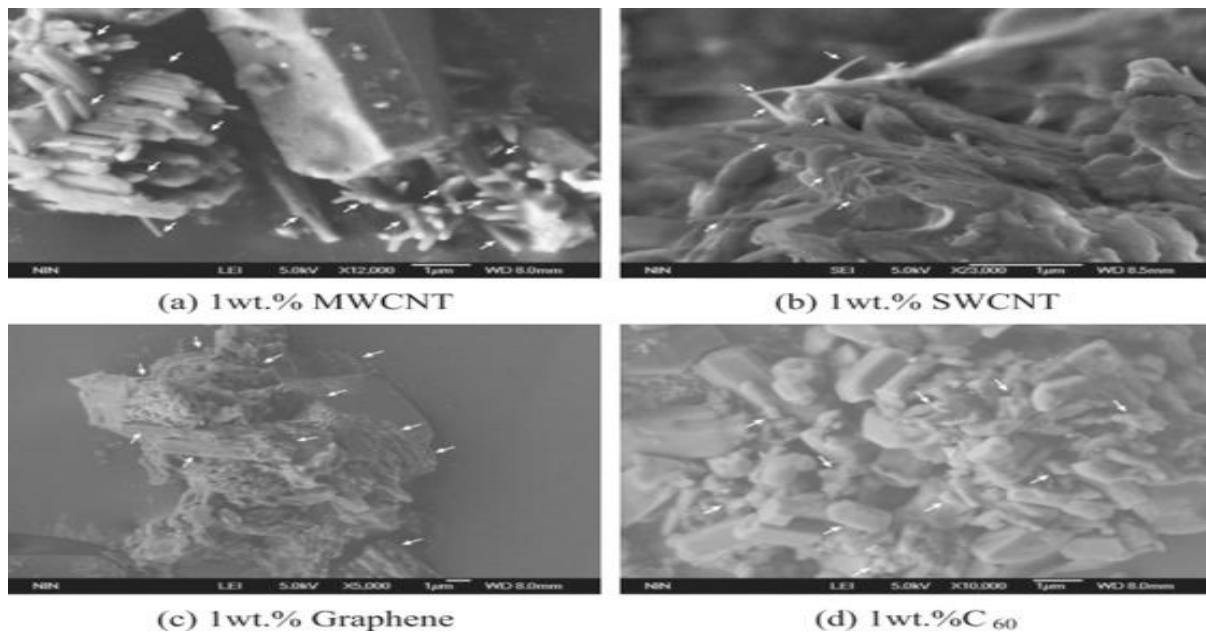


Fig.2. SEM images of salt composites with different carbon nanomaterials (Y.B. Tao, C.H. Lin, Y.L. He, 2015).

Lingyu Zheng, Xuelai Zhang, Weisan Hua, Xinfeng Wu and Fa Mao (2021) studied the effect of hydroxylated MWCNTs on the properties of Peg-CaCl₂ form-stable PCMs. It was found that 1.5% composite showed 291.30% enhancement in thermal conductivity than pure PEG1500, CaCl₂.

3.2 Metal-based materials

Metal based materials have high thermal conductivities and are beneficial to improve thermal conductivity of PCM based LTES. Metal-based materials are chemically more reactive at higher temperatures and thus have restricted applications in medium-high temperatures. Saw Chun Lin and Hussain H. Al-Kayiem (2016) reported enhanced thermal conductivity upon incorporation of copper nanoparticles in paraffin.

In the year 2017, Zhang et al. demonstrated that the inclusion of graphene nanosheet into Li₂CO₃-Na₂CO₃-K₂CO₃ lowered the latent heat of basic PCMs. D. Dsilva et al (2018), showed that latent heat could be improved by 64.7 % and 15.7% with addition of TiO₂ and CuO into paraffin. Han et al. (2020) reported that while adding nanoparticle additives into the base PCMs to enhance the thermal conductivity, the existing of nanoparticles may either lower or enhance the latent heat depending upon the melting-solidification process, types of nanomaterials and mole fraction of nanomaterials.

Rajat Saxena, Charu Dwivedi, Viresh Dutta, *S. C. Kaushik* and Dibakar Rakshit (2020) studied low-temperature melting PCM (n-nonadecane) which has the potential to thermally regulate buildings and systems. Nano-enhanced PCMs were prepared with TiO₂ by continuous spray pyrolysis method and then dispersed in the PCM matrix. They observed 37% enhancement in thermal conductivity. Jacob Mingear, Zachary Farrell, Darren Hartl and Christopher Tabor (2021) studied the effect of Gallium-indium nanoparticles in PCMs and revealed their possible application in extreme conditions such as space applications or low temperature imaging systems.

4. Conclusion and future directions

- i. The commonly employed methods for thermal conductivity improvement are addition of porous media or nanoparticles into PCM base. Both metal nanoparticles and carbon nanoparticles are helpful to improve the thermal conductivity of PCM base.
- ii. Additives affect the natural convention of liquid PCM while melting.
- iii. Carbon nanomaterials as excellent additives as they have high thermal conductivity, low density and high stability can be achieved by increasing the aspect ratio.
- iv. Aspect ratio of different carbon nanomaterials should be taken into account as higher thermal conductivity can be achieved with larger aspect ratio.
- v. Geometrical parameters and concentration of nanomaterials also influence the thermal conductivities of PCMs.
- vi. The different preparation strategies and dispersion methods also affect the thermal conductivity enhancement in PCMs and more focus in this direction is required in future.

REFERENCES

1. Amir Al-Ahmed, Ahmet Sari, Mohammad Abu Jafar Mazumder, Gökhan Hekimoğlu, Fahad A. Al-Sulaiman & Inamuddin. (2020). Thermal energy storage and thermal conductivity properties of fatty acid/fatty acid-grafted-CNTs and fatty acid/CNTs as novel composite phase change materials. *Scientific Reports*, 10, 9168.
2. Dsilva Winfred Rufuss. D, Suganthi. L, Iniyani. S, Davies. P.A. (2018). Effects of nanoparticle-enhanced phase change material (NPCM) on solar still productivity. *J Cleaner Prod*, 192, 9-29.

3. Han.D, Guene Lougou.B, Xu.Y, Shuai.Y and Huang.X. (2020). Thermal properties characterization of chloride salts/nanoparticles composite phase change material for high-temperature thermal energy storage. *Appl Energy*, 264, 114674.
4. Jacob Mingear, Zachary Farrell, Darren Hartl and Christopher Tabor. (2021) Gallium–indium nanoparticles as phase change material additives for tunable thermal fluids. *Nanoscale*, 13, 730-738.
5. Jaguemont.J, N. Omar. N, Van den Bossche. P and Mierlo.J (2018) Phase-change materials (PCM) for automotive applications. A review *Appl Therm Eng*, 132. 308-320.
6. Saeed Ranjbar,Hamid Masoumi, Ramin Haghghi Khoshkhoo & Mojtaba Mirfendereski. (2020). Experimental investigation of stability and thermal conductivity of phase change materials containing pristine and functionalized multi-walled carbon nanotubes *Journal of Thermal Analysis and Calorimetry*, 140, 2505–2518.
7. Saw Chun Lin and Hussain H. Al-Kayiem. (2016). Evaluation of copper nanoparticles – Paraffin wax compositions for solar thermal energy storage. *Solar Energy*, 132:267-278.
8. Saxena, R., Dwivedi, C., Dutta, V. S. C. Kaushik S.C and Rakshit. D. (2021). Nano-enhanced PCMs for low-temperature thermal energy storage systems and passive conditioning applications. *Clean Techn Environ Policy* 23, 1161–1168.
9. Soha Hashempour and Mohammad Hassan Vakili. (2018). Preparation and characterisation of nano enhanced phase change material by adding carbon nano tubes to butyl stearate. *Journal of Experimental Nanoscience*, 13 (1), 188-198
10. Tao. Y.B, Lin.C. H and He Y.L. (2015). Preparation and thermal properties characterization of carbonate salt/carbon nanomaterial composite phase change material. *Energy Convers Manage*, 97, 103-110.
11. Zhang.Z, Yuan. Y, Alelyani. S, Cao.X, and Phelan.P.E. (2017). Thermophysical properties enhancement of ternary carbonates with carbon materials for high-temperature thermal energy storage. *Sol Energy*, 155, 661-669.
12. Zheng. L, Zhang..X, Hua. W, Wu. X and Mao. F. (2021). The Effect of Hydroxylated Multi-Walled Carbon Nanotubes on the Properties of Peg-Cacl2 Form-Stable Phase Change Materials. *Energie,s* 14, 1403-1405.

4. Recent Trends and Challenges of Lithium Sulphur Batteries

T.R. Heera^a and Gengan Saravanan^{b*}

^aDepartment of Chemistry, AMET University, Chennai, Tamil Nadu, India

^{b,*} Department of Chemistry, Koneru Lakshmaiah Education Foundation, Hyderabad-500075, Telangana, India. E-mail: saravanan3che@gmail.com; saravanan@klh.edu.in

Abstract

Lithium-ion (Li-ion) batteries that are currently available in market have certain limitations due to their low energy density and do not meet the growing demands of the energy storage market. Thus, building next-generation rechargeable Li and Li-ion batteries with higher energy densities, better safety characteristics, lower cost and longer cycle life is vital to overcome the challenges of fast depleting conventional energy resources. To achieve smaller and lighter next-generation rechargeable Li and Li-ion batteries that can outperform commercial Li-ion batteries, many new strategies involving different energy storage chemistries are being extensively investigated. In this review, we summarize the current trends and challenges of Li-S batteries.

Keywords: Energy storage devices, Li ion battery, Li-S battery, Alternate energy source

1. Introduction

The energy demands of the world are ever increasing and it is vital to develop energy efficient systems to overcome this global challenge. In recent years extensive research has been carried out in the development of battery technology for highly efficient energy conversion and storage. The development of cost-effective, sustainable, safe and less toxic batteries is one solution to depletion of fossil fuel resources. Further, the rechargeable battery system should be compatible with complementary technologies such as wind, solar and geo-thermal technologies in order to store the energy harvested from these non-conventional sources. The advanced lithium-ion batteries have been found to most promising devices for electrochemical energy storage compared to other conventional batteries such as lead-acid, nickel-iron and nickel– metal hydride [1,2].

The low reduction potential, the easy accommodation and fast ion mobility of Li in most solids has helped Li-ion batteries provide the highest specific energies, volumetric energy densities and highest power densities when compared to alternative metal-ion batteries. Li-ion batteries have

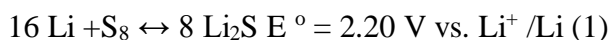
been successfully commercialized after 25 years of research and is widely used in our daily life in various applications from digital cameras to pure-electric vehicles. It is estimated that emission of greenhouse gases, noise pollution and immediate environmental pollution will be remarkably lowered if the majority of gasoline powered ground transportation is fully replaced by pure-electric vehicles in the next 10 to 20 years.

For large-scale applications in the future, in order to meet the ever-growing global market demands that the next generation rechargeable Li and Li-ion batteries need to go smaller, lighter (higher energy densities), safer, and cheaper, as long as these requirements are not mutually exclusive. There are several criteria for achieving high energy densities in next generation rechargeable Li and Li-ion batteries, but the development and modification of electrodes (high voltage cathodes and high capacity battery materials) and electrolytes lie at the heart of this technology.

This review summarizes the recent advances and current challenges of rechargeable Li-sulphur batteries as Li-S battery is the most promising technology within the Li-chalcogen chemistry.

2. Operating Principle of Lithium-Sulphur Batteries

A typical lithium-sulfur battery cell consists of metallic lithium as the negative electrode while the positive electrode is of sulfur with liquid electrolyte as both charge transfer medium and ionic conductor within the sulfur-containing cathode. Figure 1 shows the schematic configuration of a typical Li-S cell, which is based on the following conversion reaction:



Upon complete conversion, the sulfur cathode has a theoretical specific capacity of 1,675 mAh g⁻¹; and the whole Li-S cell demonstrates a theoretical energy of 2,500 Wh kg⁻¹ or 2,800 Wh L⁻¹. The ions that move between the electrodes undergo surface reactions with the electrodes and produce polysulphide ions on the surface of the cathode which reduce in size as the battery is discharged. The initial reactions produce Li₂S₈ on the surface of the cathode which transforms over time to Li₂S. The polysulphide ions are soluble in the electrolyte and this enables them to ‘shuttle’ between the two electrodes. In this shuttling process, the molecular ions become reduced in the anode into shorter polysulphide chains before moving to the cathode where they become longer chains again. Because they continually shuttle between the electrodes, they never change back into a neutral state and become useless as far as the charging and discharging mechanisms are concerned, while simultaneously reducing the number of ions which are available for facilitating

the charge and discharge cycles of the battery. The cell voltage is lower than for the lithium-ion cell and is typically about 2 V. Different electrolytes have been considered like non-aqueous organic liquid electrolytes, ionic liquid electrolytes and non-liquid electrolytes.

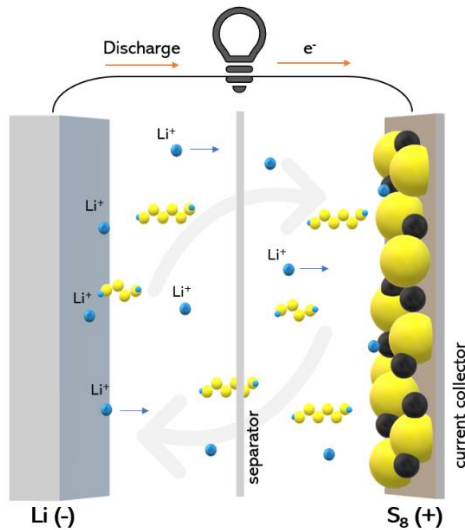


Fig1: Working principle of lithium-sulfur battery and "shuttle" effect

3. Challenges in Li-S Batteries

Among Li–chalcogen (Li–S, Li–Se and Li–Te) batteries, Li–Se and Li–Te batteries are unsuitable candidates for next-generation Li batteries due to their high cost and toxicity of Se and Te, and their lower energy densities.³ Li–S batteries has gained immense attraction among global researchers in the past ten years [3-5] S and Li₂S cathodes for Li–S batteries are undoubtedly the most promising candidates in chalcogen-based cathodes, offering the highest working potential and the highest gravimetric and volumetric capacities (1675/1166 mA h g⁻¹ and 1937 mA h cm⁻³). Li–S batteries have attracted remarkable attention from both academia and industry, in the last decade.

Lithium polysulfides as intermediate have high solubility in organic liquid electrolytes, causing polysulfide dissolution directly and a shuttle effect during cycling. Thus, during charge and discharge, S dissolves from the cathode into the liquid electrolyte, leading to capacity loss and enhanced viscosity of the electrolytes. In addition, the shuttle effect caused by soluble species (polysulfides) leads to uncontrolled interfacial deposition (re-precipitation). This results in lowered capacity and increased internal resistance of the cell due to the blocking of ionic pathways.

Moreover, as the Li–S cell continues being cycled, the liquid electrolyte becomes highly viscous due to the severe polysulfide dissolution, resulting in a lowering of the Li-ion mobility. Thus, ceaseless re-precipitation and unfavorable interactions cause thick cathode electrolyte interface and solid electrolyte interface growth on the sulfur cathode and the Li anode, respectively.

Developing high energy density Li–S batteries under low electrolyte/sulfur (E/S) ratio has a big challenge [6]. The poor wettability on thick S cathodes and the liquid consumption (side reactions) on the Li metal anode, resulting in low capacity utilization and lower cycle stability of the cells, or the death of batteries after a short cycle life (< 100 cycles) is a major challenge of low E/S [7-9].

In order to improve conductivity and hence rate capability, for suppressing the polysulfide dissolution/shuttle problem, and for realizing long-term cycle stability porous carbons is found to be good candidates. Extensive research has been carried out in their architectures, including pore size, tailored particle size, porosity, defects, pore distribution, morphology and/or surface modifications. Many investigations using graphene, N-, B- or S-doped carbons, CNTs, hierarchical porous carbons, carbon hollow spheres, MOF-derived carbons, and carbon-based flexible substrates have been studied [10-16]. Since the chemical binding energy between sulfur species and carbon is low, polysulfide dissolution and related shuttle effects cannot be fully eliminated and carbon–sulfur composites exhibit short cycle stability in standard 1 M LiTFSI-based electrolytes.

In recent years, second-generation sulfur hosts (to firmly trap sulfur species) are developed, more polar inorganic compounds viz. metallic species including transition metal sulfides, oxides, sulfides, nitrates, hydroxides, carbides, natural mineral, transition have been studied due to their relatively higher chemical binding energy to Li sulfides [17-32]. Other than these inorganic compounds, many sulfur-rich polymers have been synthesized and use strong covalent bond formation to protect S-based cathodes from polysulfide dissolution and its shuttle effects. For example, sulfur–limonene polysulfide that are cheap and eco-benign was reported to be highly promising S-based cathode for Li–S batteries, with excellent rate capability and cycle stability. Because of self-protection and the embedding of lithium sulfide and sulfur formed during the 1st cycle in the polymer matrix, polysulfide-dissolution and shuttle effects are effectively reduced. Duet al. developed a composite of monodisperse cobalt atoms embedded in nitrogen-doped

graphene (Co–N/G) metal single atoms which effectively improves the performance in high-sulfur content cathodes [33-36].

Also, many supersaturated salt–solvent mixtures were developed as a popular strategy to prevent polysulfide dissolution and its shuttle effects due to a smaller fraction of free solvent molecules for solvating the polysulfides. Kim et al. [37] showed that a new concentrated electrolyte using LiFSI instead of LiTFSI and DME solvent, offering an average CE close to 100% and high cycle stability over 1000 cycles. For the working mechanism, LiFSI induced *in situ* formation of the chemically and mechanically stable surface protection layer on both electrodes, composing an ether-based polymer with LiF on the cathode and FSI-decomposition products with LiF on the anode surfaces.

In order to fully prevent polysulfide dissolution and the related shuttle effects, all-solid-state Li–S batteries have been viewed as safe next-generation high energy batteries [38-40]. For example, combination of the designed $\text{Li}_2\text{S}@\text{C}$ nanocomposite cathode ($1.75\text{--}7.0 \text{ mg cm}^{-2}$) and promising $\text{Li}_7\text{P}_3\text{S}_{11}$ SSE offered excellent battery performance.

Conclusion

In Li–S batteries, polysulfide dissolution, shuttle effects, side reactions at the interface and continuous electrolyte consumption are the major bottlenecks. High capacity utilization, low E/S ratio and thick S (or Li_2S) cathode are vital parameters for achieving high energy Li–S batteries. Also, the capacity utilization of active sulfur is largely reduced by a low E/S ratio and thick S-based cathodes, which is due to the rather poor reaction kinetics. Within the Li–S conversion reaction chemistry, the solid to solid conversion reactions from Li_2S_4 to Li_2S_2 , and to Li_2S limit the capacity utilization. Transport at the interface between the solid and liquid should be improved to increase capacity utilization of thick cathodes under lean electrolyte conditions. One possible solution is to use dilute electrolytes such as novel electrolyte systems with lower viscosity that can provide better wetting ability instead of concentrated electrolytes. Also, the design of pore distribution host in thick electrodes with S content above 70 wt% is important to achieve both the high capacity utilization and low E/S ratio.

References:

1. N.Nitta,F.Wu,J.T.Lee and G.Yushin, Mater. Today, 2015, 18, 252–264.
2. J. M. Tarascon and M. Armand, Nature, 2001, 414, 359–36

3. X. Ji, K. T. Lee and L. F. Nazar, *Nat. Mater.*, 2009, 8, 500–506.
4. R. Kumar, J. Liu, J.-Y. Hwang and Y.-K. Sun, *J. Mater. Chem. A*, 2018, 6, 11582–11605.
5. Q. Wu, X. Zhou, J. Xu, F. Cao and C. Li, *J. Energy Chem.*, 2019, 38, 94–113.
6. W.-G. Lim, S. Kim, C. Jo and J. Lee, *Angew. Chem., Int. Ed.*, 2019, 58, 18746–18757.
7. N. B. Emerce and D. Eroglu, *J. Electrochem. Soc.*, 2019, 166, A1490–A1500.
8. E. Zhao, O. Borodin, X. Gao, D. Lei, Y. Xiao, X. Ren, W. Fu, A. Magasinski, K. Turcheniuk and G. Yushin, *Adv. Energy Mater.*, 2018, 8, 1800721.
9. L. Grande, E. Paillard, J. Hassoun, J. B. Park, Y. J. Lee, Y. K. Sun, S. Passerini and B. Scrosati, *Adv. Mater.*, 2015, 27, 784.
10. U. R. Farooqui, A. L. Ahmad and N. A. Hamid, *Renewable Sustainable Energy Rev.*, 2017, 77, 1114–1129.
11. L.-C. Zeng, W.-H. Li, Y. Jiang and Y. Yu, *Rare Met.*, 2017, 36, 339–364.
12. G.-L. Xu, J. Liu, R. Amine, Z. Chen and K. Amine, *ACS Energy Lett.*, 2017, 2, 605–614.
13. X. Gu, T. Tang, X. Liu and Y. Hou, *J. Mater. Chem. A*, 2019, 7, 11566–11583.
14. J. Jin, X. Tian, N. Srikanth, L. B. Kong and K. Zhou, *J. Mater. Chem. A*, 2017, 5, 10110–10126.
15. J. Li, C. Zhang, Y. Tao, G.-W. Ling and Q.-H. Yang, *Carbon*, 2017, 114, 752.
16. J. Xu, J. Ma, Q. Fan, S. Guo and S. Dou, *Adv. Mater.*, 2017, 29, 1606454.
17. C.-P. Yang, Y.-X. Yin and Y.-G. Guo, *J. Phys. Chem. Lett.*, 2015, 6, 256–266.
18. X. Ji, K. T. Lee and L. F. Nazar, *Nat. Mater.*, 2009, 8, 500–506.
19. R. Kumar, J. Liu, J.-Y. Hwang and Y.-K. Sun, *J. Mater. Chem. A*, 2018, 6, 11582–11605.
20. Q. Wu, X. Zhou, J. Xu, F. Cao and C. Li, *J. Energy Chem.*, 2019, 38, 94–113.
21. W.-G. Lim, S. Kim, C. Jo and J. Lee, *Angew. Chem., Int. Ed.*, 2019, 58, 18746–18757.
22. F. Wu, A. Magasinski and G. Yushin, *J. Mater. Chem. A*, 2014, 2, 6064–6070.
23. A. Abdul Razzaq, Y. Yao, R. Shah, P. Qi, L. Miao, M. Chen, X. Zhao, Y. Peng and Z. Deng, *Energy Storage Mater.*, 2019, 16, 194–202.
24. M. Zheng, Y. Chi, Q. Hu, H. Tang, X. Jiang, L. Zhang, S. Zhang, H. Pang and Q. Xu, *J. Mater. Chem. A*, 2019, 7, 17204–17241.
25. J. T. Lee, Y. Zhao, S. Thieme, H. Kim, M. Oschatz, L. Borchardt, A. Magasinski, W.-I. Cho, S. Kaskel and G. Yushin, *Adv. Mater.*, 2013, 25, 4573–4579.

25. S. Choudhury, T. Ebert, T. Windberg, A. Seifert, M. Goebel, F. Simon, P. Formanek, M. Stamm, S. Spange and L. Ionov, Part. Part. Syst. Charact., 2018, 35, 1800364.
26. F. Wu, J. T. Lee, Y. Xiao and G. Yushin, Nano Energy, 2016, 27, 238–246.
27. F. Wu, J. T. Lee, E. Zhao, B. Zhang and G. Yushin, ACS Nano, 2016, 10, 1333–1340.
28. A. Eftekhari, Sustainable Energy Fuels, 2017, 1, 14–29.
29. S. Lorger, R. E. Usiskin and J. Maier, Adv. Funct. Mater., 2019, 29, 1807688
30. Y. Song, H. Wang, Q. Ma, D. Li, J. Wang, G. Liu, Y. Yang, X. Dong and W. Yu, New J. Chem., 2019, 43, 9641–9651.
31. F. Wu, J. T. Lee, A. Magasinski, H. Kim and G. Yushin, Part. Part. Syst. Charact., 2014, 31, 639–644.
32. H. Wang, Y. Yang, Y. Liang, J. T. Robinson, Y. Li, A. Jackson, Y. Cui and H. Dai, Nano Lett., 2011, 11, 2644–2647.
33. Y. Choi, N. Yoon, N. Kim, C. Oh, H. Park and J. K. Lee, J. Electrochem. Soc., 2019, 166, A5099–A5108.
34. J. Zang, T. An, Y. Dong, X. Fang, M. Zheng, Q. Dong and N. Zheng, Nano Res., 2015, 8, 2663–2675.
35. Y. Zheng, S. Zheng, H. Xue and H. Pang, J. Mater. Chem. A, 2019, 7, 3469–3491.
36. H. Yuan, M. Zhang, C. Yang, L. Liu, R. Lu, L. Mao and Z. Wei, Macromol. Mater. Eng., 2019, 304, 1900201.
37. Y. Kim, H. Han, Y. Noh, J. Bae, M.-H. Ham and W. B. Kim, ChemSusChem, 2019, 12, 824–829.
38. Y. Liu, Y. Yan, K. Li, Y. Yu, Q. Wang and M. Liu, Chem. Commun., 2019, 55, 1084–1087.
39. L. Du, X. Cheng, F. Gao, Y. Li, Y. Bu, Z. Zhang, Q. Wu, L. Yang, X. Wang and Z. Hu, Chem. Commun., 2019, 55, 6365–6368.
40. H. Shi, S. Niu, W. Lv, G. Zhou, C. Zhang, Z. Sun, F. Li, F. Kang and Q.-H. Yang, Carbon, 2018, 138, 18–25.

5. Recent Trends in Lead-Free Inorganic Pervoskite Solar Cells: A Brief review

T.R.Heera and Gengan Saravanan

^aDepartment of Chemistry, AMET University, Chennai, Tamil Nadu, India

^{b, *} Department of Chemistry, Koneru Lakshmaiah Education Foundation, Hyderabad-500075, Telangana, India. E-mail: saravanan3che@gmail.com; saravanan@klh.edu.in

Abstract

There has been considerable increase in power conversion efficiency of organic–inorganic hybrid perovskite solar cells (PSCs) in comparison with commercially available silicon solar cells. The presence of organic compounds in perovskite solar cells has made them unstable in air. This bottleneck can be overcome by fully replacing the A-site organic cations with pure inorganic. Recent research in this area has shown significant results and the PCE of inorganic lead-based PSCs has exceeded 17%. This review paper reveals the recent developments of inorganic PSCs and its future prospects.

Keywords: Batteries, Solar photovoltaic Cell, Heavy metal batteries, Pervoskite solar cell, Alternate energy source

1. Introduction

The global increase in energy demands has led to the fast depletion of available fossil fuel resources. Development of renewable energy sources is the only possible solution to overcome this problem of depleting conventional energy resources and protect the earth from further damages due to combustion of fossil fuels. In this context, solar energy harvesting is one of the promising technologies as a clean and readily available energy source in most parts of the world. Conventional solar cells available in the market with a power conversion efficiency of 15-18% are costly due to high melting point of silicon the device fabrication at high temperature. Hence researchers have shown great interest in developing solar cells using various alternative materials as substitute to crystalline silicon. Solar cells based on natural pigments, organic polymers, quantum dots, hybrid organic/Inorganic nanocomposites, etc have been intensely studies by various research groups worldwide.

In recent years, perovskite solar cells have increased in power conversion efficiency at a phenomenal rate compared to other types of photovoltaics. Perovskite solar cells (PSCs), a new type of promising photovoltaic technology, exhibited a fast improvement in efficiency from 3.8% in 2009 to 24.2% in 2019[2–7]. The most efficient PSCs (PCE > 20%) have been constructed from organic–inorganic hybrid perovskite materials, ABX_3 , where A is an organic cation such as methylammonium (MA^+), formamidinium (FA^+) or their mixture, B is Pb^{2+} and X is Br, I or mixture of the two. However, the organic–inorganic hybrid perovskite materials lack stability when decompose on exposure to heat, oxygen, moisture and light [8–11].

The first all-inorganic PSCs were based on tin-based perovskite $CsSnI_3$, showing PCE of 0.88% in 2012 and 2.02% in 2014[12, 13]. Kulbak et al. fabricated the first $CsPbBr_3$ -based PSCs with PCE up to 5.95% and further demonstrated that the inorganic $CsPbBr_3$ perovskite can be thermally stable up to 580^0C , while the organic $MAPbI_3$ starts losing mass at about 200^0C [14,15]. The $CsPbBr_3$ inorganic PSCs also display negligible degradation in the humid ambient environment for over three months, demonstrating excellent long-term stability [16]. Mixed halide $CsPbI_2Br$ -based PSC and the first $CsPbI_3$ QDs-based PSC exhibited PCE of nearly 10% [17] and 10.77%, [18] in 2016 respectively. Various strategies such as deposition, the use of doping/additives, tuning grain size and interface engineering were investigated to enhance the efficiency and the stability of inorganic PSCs. Until now, $CsPbI_3$ has been the most promising inorganic perovskite in PSCs with PCE higher than 17% [19]. The stability issues of lead-free $CsSnI_3$ perovskite should be fully addressed in order to improve their performance.

2. Working principle of Perovskite Solar cells

Solar cells are devices that can convert solar energy into electrical energy. The sun, as the energy source, is a blackbody with a light spectrum at the temperature of about 5800 K. AM 1.5 spectrum with light intensity of 100 mW cm^2 the standard conditions for the terrestrial characterization of solar cells, corresponding to a 1.5 times longer path length of the sunlight than that when the sun is directly overhead. For the semiconductor-based photovoltaics, photons with energy greater than the band gap energy can excite the electrons from the valence band to the conduction band across the bandgap, followed by carrier extraction of both electrons and holes due to the built-in electric fields or diffusion. A semiconductor with a low bandgap can absorb more light and generate higher current, but it also affects the output voltage which is limited by the difference of quasi-Fermi levels of electrons and holes. Also, a high bandgap will limit the light absorption and the output

current. For single junction solar cells, the optimal bandgap is between 1.1 and 1.4 eV, which can achieve high efficiency of about 33% maximum.

3. Lead free inorganic perovskite solar cells

Although lead-based devices have achieved remarkable improvement in efficiency, the toxic nature of lead is a major concern. This has led to the development of new lead-free PSCs. By replacing the B-site cation from lead to tin, the properties such as energy bandgap and stability of the cesium tin halide (CsSnX_3) perovskite are changed largely. The bandgap of CsSnI_3 , CsSnI_2Br , CsSnIBr_2 and CsSnBr_3 is about 1.30, 1.40, 1.65 and 1.75 eV, [20–22] respectively, which is closer to the ideal bandgap (1.34 eV) of the Shockley–Queisser limit for photovoltaic devices comparing to that of lead-based perovskites [23]. Therefore, theoretically, tin-based perovskites are very promising materials for PSC construction. CsSnI_3 , a typical perovskite composition for PSCs with a high optical absorption coefficient (about 10^4 cm^{-1} in the visible range) [24] and low exciton binding energy (about 18 meV), exhibits a total of four phases at different temperatures. Small turbulence of oxygen or water vapour in the ambient air results in transition of phases, which is not desirable for light absorption. Also, Y- CsSnI_3 degrades to the zero-dimensional Cs_2SnI_6 due to oxidation of Sn from Sn^{2+} to Sn^{4+} .

The promising bandgap characteristics of CsSnI_3 and the improvement of PSC solution processing techniques made further researchers to investigate on CsSnI_3 [25]. It was found that the addition of tin fluoride (SnF_2) to the CsSnI_3 precursor led to reduction in the carrier density and an increase in the mobility of perovskite films, implying suppressed Sn vacancies (V_{Sn}) as well as metallic conductivity of CsSnI_3 . In addition, the density-functional-theory calculations further demonstrated that additional SnF_2 can increase the formation energy of V_{Sn} . By adding 20 mol% excess SnF_2 to the precursor for suppressing the formation of V_{Sn} and refilling V_{Sn} , the solar cells showed the best PCE of 2.02%.

According to the studies by Sabba et al. [26] the all cesium tin halide possessed low Urbach energy, revealing low structural disorder in Sn-based perovskites. Marshell et al. reported several studies on the room temperature fabrication of perovskite films and the selection of different tin halide reducing agents for CsSnI_3 PSCs [27]. They demonstrated that the CsSnI_3 perovskite films, fabricated at room temperature, possessed low defect density and, thus, these PSCs exhibited the photovoltaic effect even without the addition of excessive Sn to the precursor. By adding SnI_2 to the perovskite precursor, the device efficiency was further increased. When they coupled the

perovskite film with excess SnI_2 to the ETL of C_{60} , a positive vacuum level shift at the $\text{CsSnI}_3/\text{C}_{60}$ interface increased the V_{OC} of the devices. By incorporating with CuI and indene- $\text{C}60$ bis adduct (ICBA), the device with 10 mol% excess SnI_2 achieved the best efficiency of 2.76% at 3 mg ml⁻¹ ICBA and the highest V_{OC} value of 0.55 V at 5 mg ml⁻¹ ICBA. They further optimized the devices and demonstrated that the inverted device can show a relatively high PCE of 3.56% even without the HTL because of the formation of a thin SnCl_2 /fullerene interface.

Wang et al. [28] demonstrated the preparation of perovskite precursors by directly dissolving CsSnI_3 perovskite powders, which were synthesized from a melting-solidification method, into a mixed polar solvent without using excess SnI_2 [28]. Regarding film deposition, they reported that increasing the annealing temperature of the CsSnI_3 perovskite film can stimulate the grain growth and enhance the crystallinity. However, it may also increase the number of the grain-boundary grooves (solid-state dewetting), generate more pinholes, increase raise the V_{Sn} of the film. As a consequence, the annealing temperature of 150°C was found to be optimal for promoting the device performance. Zhu et al. [29] developed a new evaporation assisted solution (EAS) method, a two-step method, to fabricate uniform, compact and pinhole-free CsSnI_3 films, so that the current leakage and carrier recombination could be minimized. By spin-coating the $\text{SnI}_2/\text{SnF}_2$ (1: 0.3) film on the TiO_2 substrate, followed by the thermal evaporation of CsI with different thickness, a 66 nm CsI was produced and found to fulfil the high-quality film requirements. By comparing the PSCs prepared via the EAS method to the devices prepared using the normal one-step and two-step solution methods, the CsSnI_3 devices with transport layers of TiO_2 and spiro-OMeTAD achieved the PCE of 2.23%, 1.34% and 0%, respectively, demonstrating the advantage of EAS method.

Song et al. demonstrated that using hydrazine gas, a strong reducing agent and a strong base, can inhibit the formation of Sn^{4+} and enhance the efficiency [30]. Due to the strong reducing ability of N_2H_4 , it was introduced into the perovskite film by using a reducing vapour atmosphere method instead of directly adding it to the precursor to avoid reducing Sn^{2+} to the Sn metal. The perovskite film was spin-coated under the hydrazine atmosphere, which was created by spin coating hydrazine on a blank substrate for 5 minutes for vaporization. This method can largely decrease the $\text{Sn}^{4+}/\text{Sn}^{2+}$ ratio by more than 20% and reduce recombination. Therefore, the efficiency of CsSnBr_3 PSCs can be improved from about 2.36% to 2.82% with the highest PCE of 3.04%. The fabrication processes and conditions were further optimized and applied to the construction

of CsSnI_3 PSCs [31]. By controlling the CsI/SnI_2 ratio from 0.2 to 1.0 (named as 1.0- CsI/SnI_2), a ratio of 0.4 was identified as the best condition based on the combined results of a high surface coverage of the perovskite film via SEM, no observed segregation of excess SnI_2 via XRD and a high shunt resistance. The Fermi level of 0.4- CsI/SnI_2 is shallower (4.5 eV) compared to that of 1.0- CsI/SnI_2 (4.6 eV), indicating that excess SnI_2 can reduce the p-doping level of the CsSnI_3 perovskite. By further enriching the hydrazine atmosphere to reduce the formation of Sn^{4+} and suppress recombination, the CsSnI_3 device can achieve a record high PCE of 4.81% with a high JSC of 25.71 mA cm^{-2} . Compared to pure CsSnI_3 , germanium–tin alloy perovskite (CsGe0.5Sn0.5I_3) was found to be a better candidate for fabricating stable inorganic lead-free PSCs. Because of the in situ formation of the native oxide (Sn doped GeO_2) protection layer after the perovskite film was exposed to air, superior photovoltaic performance and stability of the PSCs were obtained [32].

Conclusion

The significant V_{oc} loss of tin-based lead-free inorganic PSCs, must be overcome. It is vital to reduce the intrinsic high defect density in the perovskite films. Composition tailoring and antioxidant protection should be investigated in detail to facilitate Sn^{2+} vacancy formation and suppress oxidation. Most of earlier studies on halide double perovskite-based lead-free inorganic PSCs are merely based on theoretical calculations. Thus, more experimental studies on the materials synthesis, film preparation, and device fabrication is required in this area.

Finally, the development of novel robust charge transport materials, interface modifiers, and functional additives is necessary for improving the efficiency and stability of inorganic PSCs.

Reference:

1. R. Guerrero-Lemus and L. E. Shephard, in Low-Carbon Energy in Africa and Latin America: Renewable Technologies, Natural Gas and Nuclear Energy, Springer International Publishing, Cham, 2017, pp. 149–173, DOI: 10.1007/978-3-319-52311-8_6.
2. A. Kojima, K. Teshima, Y. Shirai and T. Miyasaka, *J. Am. Chem. Soc.*, 2009, 131, 6050–6051.
3. NREL, Best Research-Cell Efficiencies, <https://www.nrel.gov/pv/assets/pdfs/best-research-cell-efficiencies-190416.pdf>.

4. P. You, Z. Liu, Q. Tai, S. Liu and F. Yan, *Adv. Mater.*, 2015, 27, 3632–3638.
5. Z. Liu, P. You, C. Xie, G. Tang and F. Yan, *Nano Energy*, 2016, 28, 151–157.
6. G. Tang, P. You, Q. Tai, R. Wu and F. Yan, *Sol. RRL*, 2018, 2, 1800066.
7. G. Tang, P. You, Q. Tai, A. Yang, J. Cao, F. Zheng, Z. Zhou, J. Zhao, P. K. L. Chan and F. Yan, *Adv. Mater.*, 2019, 31, 1807689.
8. L. Jin-Wook, K. Deok-Hwan, K. Hui-Seon, S. Seung-Woo, C. S. Min and P. Nam-Gyu, *Adv. Energy Mater.*, 2015, 5, 1501310.
9. E. Smecca, Y. Numata, I. Deretzis, G. Pellegrino, S. Boninelli, T. Miyasaka, A. La Magna and A. Alberti, *Phys. Chem. Chem. Phys.*, 2016, 18, 13413–13422.
10. N. Aristidou, I. Sanchez-Molina, T. Chotchuangchutchaval, M. Brown, L. Martinez, T. Rath and S. A. Haque, *Angew. Chem., Int. Ed.*, 2015, 54, 8208–8212.
11. J. Yang and T. L. Kelly, *Inorg. Chem.*, 2017, 56, 92–101.
12. Z. Chen, J. J. Wang, Y. Ren, C. Yu and K. Shum, *Appl. Phys. Lett.*, 2012, 101, 093901.
13. M. H. Kumar, S. Dharani, W. L. Leong, P. P. Boix, R. R. Prabhakar, T. Baikie, C. Shi, H. Ding, R. Ramesh, M. Asta, M. Graetzel, S. G. Mhaisalkar and N. Mathews, *Adv. Mater.*, 2014, 26, 7122–7127
14. M. Kulbak, D. Cahen and G. Hodes, *J. Phys. Chem. Lett.*, 2015, 6, 2452–2456.
15. M. Kulbak, S. Gupta, N. Kedem, I. Levine, T. Bendikov, G. Hodes and D. Cahen, *J. Phys. Chem. Lett.*, 2016, 7, 167–172.
16. J. Liang, C. Wang, Y. Wang, Z. Xu, Z. Lu, Y. Ma, H. Zhu, Y. Hu, C. Xiao, X. Yi, G. Zhu, H. Lv, L. Ma, T. Chen, Z. Tie, Z. Jin and J. Liu, *J. Am. Chem. Soc.*, 2016, 138, 15829–15832.
17. R. J. Sutton, G. E. Eperon, L. Miranda, E. S. Parrott, B. A. Kamino, J. B. Patel, M. T. Hořmantner, M. B. Johnston, A. A. Haghhighirad, D. T. Moore and H. J. Snaith, *Adv. Energy Mater.*, 2016, 6, 1502458.
18. A. Swarnkar, A. R. Marshall, E. M. Sanehira, B. D. Chernomordik, D. T. Moore, J. A. Christians, T. Chakrabarti and J. M. Luther, *Science*, 2016, 354, 92–95.
19. P. Wang, X. Zhang, Y. Zhou, Q. Jiang, Q. Ye, Z. Chu, X. Li, X. Yang, Z. Yin and J. You, *Nat. Commun.*, 2018, 9, 2225.
20. I. Chung, J.-H. Song, J. Im, J. Androulakis, C. D. Malliakas, H. Li, A. J. Freeman, J. T. Kenney and M. G. Kanatzidis, *J. Am. Chem. Soc.*, 2012, 134, 8579–8587.

21. D. Sabba,H. K. Mulmudi,R. R. Prabhakar, T.Krishnamoorthy, T. Baikie, P. P. Boix, S. Mhaisalkar and N. Mathews, *J. Phys.Chem. C*, 2015, 119, 1763–1767.
22. L. Peedikakkandy and P. Bhargava, *RSC Adv.*, 2016, 6, 19857–19860.
23. K. Shum, Z. Chen, J. Qureshi, C. Yu, J. J. Wang,W. Pfenninger, N. Vockic, J. Midgley and J. T. Kenney,*Appl. Phys. Lett.*, 2010, 96, 221903.
24. Chen, C. Yu, K. Shum, J. J. Wang, W. Pfenninger,N. Vockic, J. Midgley and J. T. Kenney, *J. Lumin.*, 2012,132, 345–349.
25. M. H. Kumar, S. Dharani, W. L. Leong, P. P. Boix,R. R. Prabhakar, T. Baikie, C. Shi, H. Ding, R. Ramesh,M. Asta, M. Graetzel, S. G. Mhaisalkar and N. Mathews, *Adv. Mater.*, 2014, 26, 7122–7127.
26. D. Sabba,H. K. Mulmudi,R. R. Prabhakar, T.Krishnamoorthy,T. Baikie, P. P. Boix, S. Mhaisalkar and N. Mathews, *J. Phys.Chem. C*, 2015, 119, 1763–1767.
27. K. P. Marshall, R. I. Walton and R. A. Hatton, *J. Mater.Chem. A*, 2015, 3, 11631–11640.
28. N. Wang, Y. Y. Zhou, M.-G. Ju, H. F. Garces, T. Ding,S. P. Pang, X. C. Zeng, N. P. Padture and X. W. Sun, *Adv. Energy Mater.*, 2016, 6, 1601130.
29. P. Zhu, C. Chen, S. Gu, R. Lin and J. Zhu, *Sol. RRL*, 2018,2, 1700224.
30. T.-B. Song, T. Yokoyama, C. C. Stoumpos, J. Logsdon, D. H.Cao, M. R. Wasielewski, S. Aramaki and M. G. Kanatzidis, *J. Am. Chem. Soc.*, 2017, 139, 836–842.
31. T.-B. Song, T. Yokoyama, S. Aramaki and M. G. Kanatzidis, *ACS Energy Lett.*, 2017, 2, 897–903.
32. Q. Tai, X. Guo, G. Tang, P. You, T.-W. Ng, D. Shen, J. Cao,C.-K. Liu, N. Wang, Y. Zhu, C.-S. Lee and F. Yan, *Angew. Chem., Int. Ed.*, 2019, 58, 806–810.

6. Waste Management Risks and Opportunities Identification

Kumar S.*¹, Sivakumar K.K.² and Senthil A.²

*¹Department of Mechanical Engineering, Wollega University, Ethiopia.

²Department of Chemistry, AMET Deemed to be University, Chennai.

Abstract

Rising amount of generated waste is an increasing concern for the future generation potentially at higher risk. The purpose of this research is to identify the risks and opportunities associated with waste management practices in Malaysian University, Malaysia as per requirements under ISO 9001:2015 Clause 6.1. Using Risk-Based Thinking (RBT), Preliminary Risk Assessment (PRA) and SWOT Analysis, this research analyzed the hazardous events of managing Municipal Solid Waste (MSW) and Hazardous Waste (HW). The risks associated with MSW divided into 5 categories; human damage, climate pollution, soil, air and water contamination. Whereas, HW risks US EPA characteristics were ignitable, corrosive, reactive and toxic. The findings presented in Risk Matrix (High, Medium or Low level), revealed that the top ranking risk for MSW was fatal diseases and misplacing SW4 for HW. The research recommended more ground works in RBT application as it involves thorough look at workplace to establish a most-to-least-critical importance ranking.

Keywords: Hazardous Waste, ISO 9001:2015, Municipal Solid Waste, Risk-Based Thinking

Introduction

Poor garbage waste management is a sore to the eye and not only affects the nature aesthetic value but economy as well. Improper waste dumping comes with really harmful effects, some of which may be felt earlier while others take time. In 2017, Malaysian Government launched Green-Blue Packaging (GB). The aim of this initiative was to ensure that polythene food containers are replaced, having been observed to be non-biodegradable. With toxic chemicals associated with these containers, the initiative strived to minimize environmental pollution (that had come in the form of sewerage and drainage system choking) [2]. In order to attain the objectives of the National Waste Management strategies, the cornerstone of a quality organization is an effective Quality

Management System (QMS). ISO 9001 is the most widely used and recognized standard for QMS internationally [4]. In 2017, there came the QMS, which was an alternative version to the Malaysian Standard MS ISO 9001:2015. Governed by the Department of Standards Malaysia (DSM), this version replaced ISO 9001:2008, a former version. Regarding the process of organizing accreditation and certification, the Standard and Industrial Research Institute of Malaysia (SIRIM) plays an important and leading role towards the implementation of these procedures. Notably, QSM called for the implementation of Clause 6.1, which requires that Risk-Based Thinking (RBT) is adopted. Particularly, the clause provides room for the implementation of several actions through which opportunities and risks are addressed. Also, the actions are expected to be proportionate to the impact that they are likely to have on product and service conformity. Poor garbage waste management is a sore to the eye and not only affects the nature aesthetic value but economy as well. Improper waste dumping comes with really harmful effects, some of which may be felt earlier while others take time.

In 2017, Malaysian Government launched Green-Blue Packaging (GB). The aim of this initiative was to ensure that polythene food containers are replaced, having been observed to be non-biodegradable. With toxic chemicals associated with these containers, the initiative strived to minimize environmental pollution (that had come in the form of sewerage and drainage system choking) [2]. In order to attain the objectives of the National Waste Management strategies, the cornerstone of a quality organization is an effective Quality Management System (QMS). ISO 9001 is the most widely used and recognized standard for QMS internationally [4].

Imperative to highlight is that formal methods through which risk management systems could be documented (or implemented) are not accounted in the ISO 9001:2015 standard [1]. Risk is uncertainty that matters and may impact any of product or service objectives. This impact can be positive (opportunities) and negative (threats). The Chinese word, for risk is signifying “danger” and “opportunity” [3]. Referring to ISO 9001:2015 Clause 6.1, the new requirement RBT requires organizations to ensure that opportunities and risks that are likely to pose negative or positive effects on management system performance and operation are identified. Technically, the forecasting by practicing risk management: identification, assessment, prioritization and planning precautionary actions to mitigating or avoiding the risks. The main problem faced by organizations was ISO 9001:2015 does not prescribe a risk methodology which means they are free to adopt their own approach. The intent was that each organization assessing their own unique risks and

opportunities. In other words, “is to do whatever is right for your business”. It is also notable that there exist different methodologies but for the case of ISO 9001:2015, formal risk management is not necessary; neither does this methodology emphasize specific approaches for achieving risk identification and the documentation of the results. It is up to each organization to determine the extent of documentation needed to provide objective evidence of the RBT application. Moreover, the multiplicity of sources and methods makes it difficult to compile one compact and efficient preventive action process [7].

Objectives of the study

Since many concerns have been raised about the challenges of no standardization in new revised QMS, this research applying RBT approach as required in MS ISO 9001:2015. The objective in this research was to identify the risks and opportunities associated with waste management practices in the Malaysia TVET Institution.

Methodology and Procedure

Research background: Notably, this study is limited in a certain way. In particular, the aspect of Quality Management Team (QMT) may be interacted by following the procedure of government protocol and not the ISO business practice guidelines. Assumptions were the QMT had high level of environmentally awareness and practicing proper waste management on daily basis. The interest of these parties is seen to lie in idea generation but the enforcement of the perceived orders remains questionable and relatively wanting. This study’s research context was a TVET organization. The choice of this institution was based on training workshops that it holds relative to industrial skills; especially on subjects such as hazardous waste and municipal solid waste disposal. Indeed, the institution, through these workshops, gains exposure to different subjects on risks such as leachate, gaseous, bugs, infections, toxic effects and injuries from improper waste management. Research Location: Imperatively to note is that the specific area that was chosen to gain data entailed a public vocational institute. Specifically, information was gained from a public TVET institution. The Ministry of Human Resources Malaysia (MOHR) was in charge of this institution. Founded in 1964, the organization rests on 13.7 acres of land. Geographically, it lies 3°05'33.1"N, 101°41'13.5"E in Kuala Lumpur's Kuchai Lama area (see Figure 1). With 577 students and a staff of 182 individuals, 12 courses are offered in the institution (by 2018) [5].

Conclusion

Rising amount of generated waste is an increasing concern for the future generation potentially at risk. The purpose of this research was to identify the risks and opportunities associated with waste management practices in Malaysia TVET Institution as per requirements under ISO 9001:2015 Clause 6.1. Using Risk-Based Thinking (RBT), Preliminary Risk Assessment (PRA) and SWOT Analysis, this research analyzed the hazardous events of managing Municipal Solid Waste (MSW) and Hazardous Waste (HW). The risks associated with MSW divided into 5 categories; human damage, climate pollution, soil, air and water contamination. Whereas, HW risks US EPA characteristics were ignitable, corrosive, reactive and toxic. The findings presented in Risk Matrix (High, Medium or Low level), revealed that the top ranking risk for MSW was fatal diseases and misplacing SW4 for HW. The research recommended more ground works in RBT application as it involves thorough look at workplace to establish a most-to-least-critical importance ranking.

REFERENCES

1. Aseel M. Aljeboree , A.N.A., Adsorption of Pharmaceuticals as emerging contaminants from aqueous solutions on to friendly surfaces such as activated carbon: A review J. Pharm. Sci. & Res. , 2018. 10(9): p. 2252-2257
2. J.L. Tambosi, L.Y.Y., H.J.J.R. de Fatima Peralta Muniz Moreira, H.F. Schroder, Recent research data on the removal of pharmaceuticals from sewage treatment plants (STP). Quim Nova, 2010. 33: p. 411-420.
3. Aseel Musthaq Aljeboree, A.N.A., Colorimetric Determination of phenylephrine hydrochloride drug Using 4-Aminoantipyrine: Stability and higher sensitivity J. Pharm. Sci. & Res., 2018 10(7): p. 1774-1779
4. Jones, O.A., J.N. Lester, and N. Voulvoulis, Pharmaceuticals: a threat to drinking water? Trends in Biotechnology, 2005. 23(4): p. 163-167.
5. Aseel M. Aljeboree, A.S.A., Removal of Pharmaceutical (Paracetamol) by using CNT/ TiO₂ Nanoparticles, Journal of Global Pharma Technology, 2019. 11 (01): p. 199-205.
6. Stackelberg, P.E., et al., Persistence of pharmaceutical compounds and other organic wastewater contaminants in a conventional drinking-water-treatment plant. Science of The Total Environment, 2004. 329(1): p. 99-113.

7. Sivakumar K.K. et al., ZnO/UV induced photocatalytic degradation of textile dye, Research J Chemistry and Environment, 2021, 25(5), 2021, 160-165.
8. Aljeboree, A.M., A. N. Alshirifi, et al., "Kinetics and equilibrium study for the adsorption of textile dyes on coconut shell activated carbon, Arabian Journal of Chemistry, 2012. 10: p. S3381-S3393.
9. Alkaim AF, A.A., Alrazaq NA, Baqir S.J, Hussein F.H and Lilo AJ, Effect of pH on Adsorption and Photocatalytic Degradation Efficiency of Different Catalysts on Removal of Methylene Blue. Asian Journal of Chemistry, , 2014. 24(26): p. 8445-8448.
10. AM, A., Adsorption of crystal violet dye by Fugas Sawdust from aqueous solution. International Journal of Chem Tech Research. 9(3): p. 412-423.
11. Abdulrazzak, F.H., Enhance photocatalytic Activity of TiO₂ by Carbon Nanotubes. International Journal of ChemTech Research, 2016. 9(3): p. 431-443
12. AF Alkaim, T.K., FH Hussein, R Dillert, DW Bahnemann, Solvent-free hydrothermal synthesis of anatase TiO₂ nanoparticles with enhanced photocatalytic hydrogen production activity. Applied Catalysis A: General 2013. 466 p. 32-37.
13. Tarek A. Kandiel, L.R., Ayad Alkaim and Detlef Bahnemann, Brookite versus anatase TiO₂ photocatalysts: phase transformations and photocatalytic activities†. Photochemical & Photobiological Sciences, 2013. 12: p. 602.
14. M. R. Hoffmann, S.T.M., W. Y. Choi and, E.a.o.s. D. W. Bahnemann, and C.R. photocatalysis, 1995, 95, 69–96., Environmental applications of semiconductor photocatalysis Chem. Rev, 1995. 95: p. 69–96.
15. K. Hashimoto, H.I.a.A.F., TiO₂ photocatalysis:a historical overview and future prospects. J. Appl.Phys., 2005. 44: p. 8269–8285.
16. M. P. Finnegan, H.Z.Z.a.J.F.B., Phase stability and transformation in titania nanoparticles in aqueous solutions dominated by surface energy. J. Phys.Chem. C 2007. 111.: p. 1962–1968.
17. T. A. Kandiel, R.D.a.D.B., Titanium dioxide nanoparticles and nanostructures. Curr. Inorg.Chem., 2012. 2: p. 94–114.
18. Banfield, H.Z.Z.a.J.F., Understanding polymorphic phase transformation behavior during growth of nanocrystalline aggregates: insights from TiO₂. J. Phys. Chem. B,, 2000. 104: p. 3481–3487.

19. Hussein A.F. Photocatalytic degradation of EDTA by using TiO₂ suspension, Int. J. Chem. Sci., 2012. 10(1): p. 586-598.
20. H. Wang, C. Xie, W. Zhang, S. Cai, Z. Yang, and Y. Gui, Comparison of dye degradation efficiency using ZnO powders with various size scales. J. Hazard Mater., 2007. 141(3): p. 645-652.
21. J. Kaur, and S. Singhal, Heterogeneous photocatalytic degradation of rose bengal: Effect of operational parameters. Physica B, 2014. 450: p. 49-53.
22. M. S. Mashkour, A. F. Alkaim, L. M. Ahmed, and F. H. Hussein, Zinc oxide assisted photocatalytic decolorization of reactive red 2 dye. Int. J. Chem. Sc., 2011. 9(3): p. 969-979.
23. T. Sauer, G. C. Neto, H.J. José, and R.F. Moreira, Kinetics of photocatalytic degradation of reactive dyes in a TiO₂ slurry reactor. J. Photochem. Photobiol. A, 2002. 149: p. 147-154.
24. Aseel M. Aljeboree, H.Y.A.-G., Mohammed H. Said and Ayad F. Alkaim, The Effect of different parameters on the removal of Vitamin B12 drug (as a model biochemical pollutants) by Activated Carbon/Clay, Biochem. Cell. Arch. , 2019. 19(1): p. 000-000.
25. Miao J, J.Z., Lu HB, Habibi D and Zhang L, , Heterogeneous photocatalytic degradation of mordant black 11 with ZnO nanoparticles under UV-Vis light. Journal of the Taiwan Institute of Chemical Engineers, 2014. 45: p. 1636-1641
26. Aseel M. Aljeboree, A.F.A., Ali loay, Photocatalytic Degradation of Textile Dye Cristal Violet Wastewater using Zinc Oxide as a Model of Pharmaceutical Threat Reductions. Journal of Global Pharma Technology, 2019. 11(3): p. 138-143.

7. A Brief Review on Applications of Ultrasonic Technology in Food Quality Control

T.R.Heera^a and Gengan Saravanan^{b,*}

^aDepartment of Chemistry, AMET (Deemed to be University), Chennai, Tamil nadu

^bDepartment of Chemistry, KL University, Vijayawada

Abstract

A sound wave with frequency beyond the limit of human hearing is known as ultrasound. Tuning of ultrasound frequency has widespread applications in many industries including food. The simplicity and low cost and eco-friendly features make ultrasound techniques an emerging technology for probing and modifying the quality of food products. In last decade, ultrasound technology has shown significant processing option and replaced the conventional thermal approaches. Low power (high frequency) ultrasound is used for monitoring the composition and physicochemical properties of food components and products during processing and storage, which is vital for controlling the food properties and enhancing food quality. This brief review summarizes some of the major applications of low power ultrasound in food technology. These applications include meat products, vegetables and fruits, cereal products, aerated foods.

Keywords: Ultrasonic technology, Ultrasound frequency, Food preservation technology, Non destructive texture analysis.

1. Introduction

The sound waves having frequency that exceeds the hearing limit of the human ear (~20 kHz) are called as ultrasound. Animals like dolphins and bats make use of ultrasound for navigation/hunting utilizing the information carried by back-scattering sound waves. The human ability to minimize processing, maximize quality and ensure the safety of food products has increased manifold by adopting ultrasonic technology. Ultrasound plays an important role enhancing food processing and manipulation of texture and food analysis [1].

Depending on frequency range, the applications of ultrasound in food processing, analysis and quality control can be categorized into low and high energy. Low energy (low power, low intensity) ultrasound has frequencies higher than 100 kHz at intensities below 1 W·cm², which can

be employed for non-invasive analysis and monitoring of various food materials during processing and storage in order to achieve high quality and food safety. Low power ultrasound has been used to nondestructively incorporate genetic improvement programs for livestock and for investigating the composition of raw and fermented meat products, fish and poultry. It is also used for the quality control of fresh vegetables and fruits in both pre- and postharvest, cheese during processing, commercial cooking oils, bread and cereal products, bulk and emulsified fat based food products etc.



Figure 1: Application of Ultrasonic Technology in Food Quality Control

Ultrasonic equipment consists of three main components such as a transducer, electrical power generator and sound emitter devices. The waves are sent to the ultrasonic medium by the emitter. Two major types of ultrasonic systems are prevalent in industries. One employs a bath as in traditional method and the other uses a horn as a sound emitter. The horn based system is typically used in many applications of food processing industries.

2. Role of low power ultrasound (LPU) in food technology

2.1 Fruits and vegetables:

Ultrasonication is used to maintain both pre- and post-harvest quality attributes in fresh fruits and vegetables and is considered a substitute for washing of fruit and vegetable in food industry. In an attempt to meet the customers' requirements of not only maintaining but also improving the

nutritional value of fruit juices, ultrasonication has proved to be one such technique and is reported to retain fresh quality, nutritional value, and microbiological safety in guava juice orange juice, and tomato juice [2, 3]. Ultrasound treatment can also be used to recover the nutrient loss occurred during blanching, resulting in achieving the collaborative benefit of both the techniques. Ultrasonication cleaners (20–400 kHz) have been efficiently used to produce fruits and vegetables free of contamination and at 40 kHz, it has been Cao et al [4] applied on strawberry fruits in which decay and infection was considerably reduced along with quality maintenance. Fruits and vegetables are extremely attenuating materials due to the scattering of sound from voids and pores. This in turn makes the interpretation of ultrasound data difficult. Mizrach explained the various physiological and physiochemical changes taking place during growth and maturation, and in the course of the harvest period, storage and shelf-life. The indirect assessment of the proper harvesting time, storage period or shelf-life was obtained from the results of ultrasound measurements and other physiochemical measurements, such as firmness, mealiness, dry weight percentage (DW), oil contents, total soluble solids (TSS), and acidity. Studies revealed that the amplitude of the ultrasound wave transmitted through fruit peels enhanced when the color changed from green to yellow indicating a good correlation between the ripeness and the acoustic attenuation. Also, the maturity and sugar content of plum fruits estimated by measuring ultrasound attenuation in the fruit tissue correlated well with the firmness of plums and that of tomato in other study. This reveals the importance of using the attenuation parameter, which has also been used earlier for detecting defective potatoes. Sankarappa and coauthors measured the density and ultrasonic velocity at a frequency of 3 MHz in some refined and unrefined edible oils of groundnut, coconut, castor, sunflower and safflower which allowed to estimate various physical parameters such as adiabatic compressibility, specific volume, molar sound velocity, molar compressibility and intermolecular free length [5]. The effects of a ultrasound treatment on the organoleptic characteristics and nutritional quality of mango were studied by valente etal and showed that the treatment preserves the consistency, colour, and content of the carotenoid phenols and ascorbic acid as well as the control product [6,7].

2.2 Cereal products

Bread, biscuits, breakfast bars and other bakery products are some of the important food products obtained from cereals. A study to examine the extent of mixing on three different flour dough systems using ultrasound and conventional rheology technique showed strong correlations

between ultrasound parameters (velocity and attenuation) and rheology, which indicated the possibility of using ultrasound for on-line dough quality control [8]. Earlier researchers have reported on ultrasound velocity technique to monitor changes in wheat flour dough consistency induced by proteins and gelatinization of the starch [9]. A low frequency acoustic method was developed to estimate the structural and mechanical properties of cereal products such as wafer sheets, crisp bread, crackers and ring-shaped rolls from the magnitude of the amplitude of a penetrated acoustic signal [10]. Good correlations were found between penetrated acoustic signals and the structural and mechanical properties (density, surface porosity, mechanical strength) of porous food products, measured by a traditional method. Many food products are made with batter such as pancakes, cupcakes, waffles, doughnut, tempura, etc. Ultrasound techniques are used to monitor the physical properties of batters (density, viscosity and rheology) and cakes (volume, symmetry, volume index, height and density). Fox et al. (2004) [11]. Ultrasound measurements show significant correlations between the acoustic impedance and the batter consistency [12].

2.3 Meat products

In the beef industry, LPU has been a fast, reproducible and reliable technology to improve genetic improvement programs for livestock [13]. As same as for human pregnancy, sound waves of various frequencies (depending on depth of tissue penetration and resolution) produce vibration–reflection images of tissues such as muscle, fat, and internal organs in live animals, which can be used as a management tool in selection and replacement of breeding stock for the improvement of the genetics of the herd. Using a frequency scanning pulse echo reflectometer (FSPER), they studied the temperature dependency of the sound velocity of fish analogs having various concentrations of solids-non-fat, water, and oil. They treated the fish composition as (solids-non-fat +water) and an oil phase, and developed an important relationship between the ultrasound velocity values at a constant temperature and the volume fractions of the two components, which gave excellent correlation between the values predicted and the actual measured values[14]. The same method was later used to determine the composition of chicken analogs and the solid fat content of chicken fat suggesting the advantages of LPU as a rapid and nondestructive method in food analysis. Sonication is used to tenderize meat by releasing myofibrillar proteins from muscle cells and increase the water-binding capacity and cohesion of the meat.

Utilizing sound energy (changing sound energy to heat) can speed up meat thawing yet yielding no significant differences in microbiological, and chemical properties compared with the

meat immersed in water (meat thawed by water). Meat quality is improved by applying ultrasound to reducing meat brining time. Basically, when the dynamics of the sound wave (high than sound detected by human ears) are applied in ultra-sonication physics (mechanical waves: compression and rarefaction) under controlled conditions (ultrasound cavitation) to generate high temperature and pressure by cavitation bubbles, quality food will be yielded based on the desired frequency range utilized[15-19].

Meat Product	Measurements	Advantage
Livestock, beef cattle carcass, sheep carcass, carcass traits of Bali bulls, growing lambs	Fat and muscle accretion and body composition, intramuscular fat (IMF) percentage, and carcass traits, degree of muscle development	Enhance genetic improvement programs for livestock; quality control of meat
Pigs	Characterize and classify back fat from animals of different breeds and feeding regimes	Quality control; improve meat quality traits in breeding animals
Chicken	Composition of chicken analogs; solid fat content	Nondestructive and rapid detection; alternative to x-ray methods.
Skinless poultry breast	Defects and internal objects	Quality control
Fermented meat	Quality determination	Quality control

Table 1: Applications of low power ultrasound in analysis and quality control of meat products

2.4 Fat and emulsion products

Ultrasonication is relatively cheaper technique for emulsion formation with significant effect on emulsion droplet size and structure. In ultrasonic emulsification application of high energy reported viscosity decrease and lesser particle size distribution in sub-micron oil-droplets emulsions. However, change in sonication parameters caused remarkable change in stability and oil droplet size of the emulsion formed.

The solid fat content (SFC) of food products containing significant amounts of fats (e.g., chocolate, butter, margarine, shortening and creams) determines many of the sensory attributes such as texture and mouthfeel [20]. Thus, SFC determination is an essential analytical procedure to ensure the product quality during processing. SFC is traditionally measured by pulsed field nuclear magnetic resonance technique (p-NMR). Ultrasonic measurements accurately described the SFC variation, and the two techniques can be used as on-line methodologies to determine SFC during the crystallization of fats. Ultrasonic characterization of fluid properties depends on the physical measurement of the ultrasonic wave attenuation coefficient and/or phase velocity as functions of frequency [21].

McClements and Coupland applied themultiple scattering theory to obtain the mean droplet diameter and droplet size distribution in oil-in-water (O/W) emulsions [22-24]. Ultrasonic velocity measurements also employed to find out other physical properties of O/W emulsions such as disperse phase volume fraction, solid fat content.

2.5 Aerated foods

Aerated foods contain air bubbles distributed in a viscoelastic liquid or solid matrix such as ice cream, whipped cream, confectionary, bread dough and desserts. The quality of whipped products of the food industry is closely linked to the characteristics of the dispersed gas phase, such as the bubble morphology, the mean bubble size and the uniformity of the bubble size distribution [25]. Because aerated foods are optically opaque or have delicate structures that are easily damaged, there is a lack of analytical techniques capable of providing information about bubble characteristics in aerated foods. It is known that air bubbles modify the propagation of sound and cause high attenuation to sound waves and prevent their transmission. Tests between 300 kHz and 2.25 MHz confirmed the difficulty of transmitting ultrasound through cake batters as they were mixed over the normal range of low cost transducers due to bubbles.

Fox et al. [26] then designed a low cost ultrasound probe with 15 mm diameter transducer (2.25 MHz) to obtain measurements in reflection, which allowed monitoring the specific gravity of batter as indicator of quality and progress of the mixing process. The bubble size distribution in dough was investigated over a wide frequency range [27]. The studies revealed that the bubble concentration in dough and the time after mixing influenced the shape and position of the velocity and attenuation peaks. Ultrasonic spectroscopy was employed to characterize a model aerated food system consisting of agar gel in which both bubbles and polystyrene beads are embedded found a good correlation between ultrasound and image analysis [28].

3. Conclusion

Ultrasound is a promising technology in food science and technology. The tunable frequency of ultrasound diversified its applications in the areas of food analysis, processing and quality control. The application of low power (high frequency) ultrasound provides a non-invasive, economic and simple techniques useful for estimating the food composition of fish, eggs, dairy, etc. and monitoring physicochemical and structural properties and investigating contamination by metals and other foreign materials in canned food, dairy products, etc. Monitoring the composition and physicochemical properties of food during processing and storage is important for the production of food products with high performance, quality and stability. A lot of research has been conducted on ultrasound technologies in food technology, but still a great deal of future research is necessary in order to produce industrial-automated ultrasound systems that will help in reduction of labor, cost, energy, and should ensure the maximum production of high value and safe food products.

REFERENCES

1. Knorr, D., Froehling, A., Jaeger, H., Reineke, K., Schlueter, O., & Schoessler, K. (2011). Emerging technologies in food processing. *Annual Review of Food Science and Technology*, 2, 203–235.
2. McClements, D. J., & Gunasekaran, S. (1997). Ultrasonic characterization of foods and drinks: Principles, methods, and applications. *Critical Reviews in Food Science and Nutrition*, 37(1), 1–46.

3. Mizrach, A. (2008). Ultrasonic technology for quality evaluation of fresh fruit and vegetables in pre- and postharvest processes. *Postharvest Biology and Technology*, 48(3), 315–330.
4. Cheng, Y., & Haugh, C. G. (1994). Detecting hollow heart in potatoes using ultrasound. *Transactions of the Asae*, 37(1), 217–222.
5. Sankarappa, T., Kumar, M. P., & Ahmad, A. (2005). Ultrasound velocity and density studies in some refined and unrefined edible oils. *Physics and Chemistry of Liquids*, 43(6), 507–514.
6. Valente, M.; Prades, A.; Laux, D. Potential use of physical measurements including ultrasound for a better mango fruit quality characterization. *J. Food Eng.* 2013, 116, 57–64.
7. Santos, J.G.; Fernandes, F.A.N.; de Siqueira Oliveira, L.; de Miranda, M.R.A. Influence of ultrasound on fresh-cut mango quality through evaluation of enzymatic and oxidative metabolism. *Food Bioprocess. Technol.* 2015, 8, 1532–1542.
8. Ross, K. A., Pyrak-Nolte, L. J., & Campanella, O. H. (2004). The use of ultrasound and shear oscillatory tests to characterize the effect of mixing time on the rheological properties of dough. *Food Research International*, 37(6), 567–577.
9. García-Álvarez, J., Salazar, J., & Rosell, C. M. (2011). Ultrasonic study of wheat flour properties. *Ultrasonics*, 51(2), 223–228.
10. Juodeikiene, G., & Basinskiene, L. (2004). Non-destructive texture analysis of cereal products. *Food Research International*, 37(6), 603–610.
11. Fox, P., Smith, P. P., & Sahi, S. (2004). Ultrasound measurements to monitor the specific gravity of food batters. *Journal of Food Engineering*, 65(3), 317–324.

12. Gómez, M., Oliete, B., García-Álvarez, J., Ronda, F., & Salazar, J. (2008). Characterization of cake batters by ultrasound measurements. *Journal of Food Engineering*, 89(4), 408–413.
13. Crews, D. H., Jr., & Kemp, R. A. (2002). Genetic evaluation of carcass yield using ultrasound measures on young replacement beef cattle. *J. Anim Sci.*, 80(7), 1809–1818.
14. Ribeiro, F. R. B., Tedeschi, L. O., Stouffer, J. R., & Carstens, G. E. (2008). Technical note: A novel technique to assess internal body fat of cattle by using real-time ultrasound. *J. Anim Sci.*, 86(3), 763–767.
15. Silva, S. R., Afonso, J. J., Santos, V. A., Monteiro, A., Guedes, C. M., Azevedo, J. M. T., et al. (2006). In vivo estimation of sheep carcass composition using real-time ultrasound with two probes of 5 and 7.5 MHz and image analysis. *Journal of Animal Science*, 84(12), 3433–3439.
16. Theriault, M., Pomar, C., & Castonguay, F. W. (2009). Accuracy of real-time ultrasound measurements of total tissue, fat, and muscle depths at different measuring sites in lamb. *Journal of Animal Science*, 87(5), 1801–1813. (Theriault, Pomar, & Castonguay, 2009).
17. Ghaedian, R., Coupland, J. N., Decker, E. A., & McClements, D. J. (1998). Ultrasonic determination of fish composition. *Journal of Food Engineering*, 35(3), 323–337. Ghaedian, Coupland, Decker, & McClements, 1998;
18. Ghaedian, R., Decker, E. A., & McClements, D. J. (1997). Use of ultrasound to determine cod fillet composition. *Journal of Food Science*, 62(3), 500–504.
19. Chanamai, R., & McClements, D. J. (1999). Ultrasonic determination of chicken composition. *Journal of Agricultural and Food Chemistry*, 47(11), 4686–4692. (Chanamai & McClements, 1999).
20. Martini, S., Awad, T. S., & Marangoni, A. G. (2006). Structure and properties of fat crystal networks. In F. Gunstone (Ed.), *Modifying food lipids for use in foods* (pp. 349–380). Cambridge, U.K: Woodhead Publishing Ltd. Martini et al., 2006).
21. Challis, R. E., Povey, M. J. W., Mather, M. L., & Holmes, A. K. (2005). Ultrasound techniques for characterizing colloidal dispersions. *Reports on Progress in Physics*, 68(7), 1541–1637.
22. McClements, D. J. (2005). *Food emulsions: Principles, practices, and techniques*. CRC.

23. McClements, D. J., & Coupland, J. N. (1996). Theory of droplet size distribution measurements in emulsions using ultrasonic spectroscopy. *Colloids and Surfaces A: Physicochemical and Engineering Aspects*, 117(1–2), 161–170.
24. McClements, D. J., Dickinson, E., & Povey, M. J. W. (1990). Crystallization in hydrocarbon-in-water emulsions containing a mixture of solid and liquid droplets. *Chemical Physics Letters*, 172(6), 449–452.
25. Labbafi, M., Thakur, R. K., Vial, C., & Djelveh, G. (2007). Development of an on-line optical method for assessment of the bubble size and morphology in aerated food products. *Food Chemistry*, 102(2), 454–465.
26. Fox, P., Smith, P. P., & Sahi, S. (2004). Ultrasound measurements to monitor the specific gravity of food batters. *Journal of Food Engineering*, 65(3), 317–324.
27. Leroy, V., Fan, Y., Strybulevych, A. L., Bellido, G. G., Page, J. H., & Scanlon, M. G. (2008). Investigating the bubble size distribution in dough using ultrasound. *Bubbles in food*, 2, 51–60.
28. Strybulevych, A., Leroy, V., Scanlon, M. G., & Page, J. H. (2007). Characterizing a model food gel containing bubbles and solid inclusions using ultrasound. *Soft Matter*, 3(11), 1388–1394.



AMET International Journal of Physical & Chemical Sciences

Published by : AMET Deemed to be University

No: 135, East Coast Road, Kanathur, Chennai - 603 112, INDIA.

Tel: 044 - 2744 4625 / 627 / 628, Fax : 044 - 27472804

University Website: www.ametuniv.ac.in

Journal Website: www.aijpcs.com

E-mail: office@ametuniv.ac.in